



Negative ion chemistry in Titan's upper atmosphere

V. Vuitton^{a,b,*}, P. Lavvas^b, R.V. Yelle^b, M. Galand^c, A. Wellbrock^{d,e}, G.R. Lewis^{d,e},
A.J. Coates^{d,e}, J.-E. Wahlund^f

^a Laboratoire de Planétologie de Grenoble, CNRS, Grenoble, France

^b Lunar and Planetary Laboratory, University of Arizona, Tucson AZ, USA

^c Department of Physics, Imperial College, London, UK

^d Mullard Space Science Laboratory, University College London, Dorking, UK

^e Centre for Planetary Sciences, University College London, London, UK

^f Swedish Institute of Space Physics, Uppsala, Sweden

ARTICLE INFO

Article history:

Received 30 October 2008

Received in revised form

4 April 2009

Accepted 9 April 2009

Available online 18 April 2009

Keywords:

Atmospheres

Composition

Ionospheres

Organic chemistry

Titan

ABSTRACT

The Electron Spectrometer (ELS), one of the sensors making up the Cassini Plasma Spectrometer (CAPS) revealed the existence of numerous negative ions in Titan's upper atmosphere. The observations at closest approach (~ 1000 km) show evidence for negatively charged ions up to $\sim 10,000$ amu/q, as well as two distinct peaks at 22 ± 4 and 44 ± 8 amu/q, and maybe a third one at 82 ± 14 amu/q. We present the first ionospheric model of Titan including negative ion chemistry. We find that dissociative electron attachment to neutral molecules (mostly HCN) initiates the formation of negative ions. The negative charge is then transferred to more acidic molecules such as HC_3N , HC_5N or C_4H_2 . Loss occurs through associative detachment with radicals (H and CH_3). We attribute the three low mass peaks observed by ELS to CN^- , $\text{C}_3\text{N}^-/\text{C}_4\text{H}^-$ and C_5N^- . These species are the first intermediates in the formation of the even larger negative ions observed by ELS, which are most likely the precursors to the aerosols observed at lower altitudes.

© 2009 Elsevier Ltd. All rights reserved.

1. Introduction

Titan has been an object of considerable scrutiny since the arrival of Cassini–Huygens in the Saturn system in July 2004. Titan is the only satellite in the solar system with an extensive atmosphere, largely composed of N_2 , with CH_4 (2%) and H_2 (0.4%) being the most abundant minor constituents (Flasar et al., 2005; Yelle et al., 2006). N_2 and CH_4 are dissociated or ionized in the upper atmosphere by solar EUV and soft X-ray radiation, and impact of supra-thermal electrons, protons and oxygen ions (Cravens et al., 2008; Lavvas et al., 2008a). The highly reactive radical and ion species produced in these processes react to form a plethora of hydrocarbons and nitrogen-bearing species that characterize Titan's atmosphere (Cui et al., 2009; Teanby et al., 2006; Vinatier et al., 2007; Vuitton et al., 2007). The presence of CO, CO_2 and H_2O (De Kok et al., 2007), which likely originate from an influx of O^+ and micrometeorite ablation (Hörst et al., 2008), complete the collection of species that exist in Titan's atmosphere. Observations by the Ion Neutral Mass Spectrometer (INMS) onboard the Cassini spacecraft showed that Titan has a complex

* Corresponding author. Present address: Laboratoire de Planétologie de Grenoble, Bâtiment D de Physique BP 53, 38041, Grenoble, France.

Tel.: +33 04 76 63 52 78; fax: +33 0 476 51 41 46.

E-mail address: veronique.vuitton@obs.ujf-grenoble.fr (V. Vuitton).

ionosphere (950–2000 km), containing a rich positive ion population of organic molecules with mass-to-charge ratios (m/q) up to a few 100 amu and a maximum total density of a few 1000 cm^{-3} (Cravens et al., 2006; Vuitton et al., 2006, 2007).

The presence of negative ions in Titan's atmosphere had only been considered for the cosmic ray-induced ionosphere that lies below 200 km. The pre-Voyager model of Capone et al. (1976) considered the formation of CH_3^- and H^- by three-body electron attachment. They calculated a negative to positive ion ratio of $\sim 10^{-4}$ in the nighttime ionosphere, which became approximately four orders of magnitude lower in the daytime ionosphere because of the high photo-detachment rate. A decade later, Borucki et al. (1987) considered the possible formation of negative ions by three-body electron attachment to radicals such as NH_2 , CH_3 , CN , C_2H and H. While CN and C_2H form relatively stable negative ions (see Section 3.1), the concentrations of these radicals, as calculated by Capone et al. (1980) and Yung et al. (1984), are too small for them to be a significant source of negative ions. Calculated equilibrium concentrations of CH_3 , NH_2 and H are larger, but the negative ions they form are far less stable against photo-detachment (see Section 3.1). Under nighttime conditions, their calculations predict that the negative to positive ion ratio is much less than 0.1.

Molina-Cuberos et al. (2000) calculated the concentration of anions based on a parametric study of the mixing ratio of a

hypothetical electrophilic species present in the lower ionosphere of Titan. They include anion production by three-body electron attachment and destruction by ion–ion recombination. With the mixing ratio (10^{-15} – 10^{-14}) of electrophilic species (H , CH_3 , C_3H_2) predicted by neutral models (Lara et al., 1996; Toublanc et al., 1995), they find a negative to positive ion ratio of less than 0.02. They also discuss the effect of electron detachment from negative ions by absorption of solar radiation.

Bakes et al. (2002) developed a model of photoelectric charging for polycyclic aromatic hydrocarbon (PAHs) macromolecules and carbonaceous sub-micrometer aerosols (radius $>10 \text{ \AA}$). PAHs are moderately electrophilic, with electron affinities typically $<1.0 \text{ eV}$. Bakes et al. (2002) consider the formation of negatively charged species by collisional charging and their loss by photo-detachment. They find that the macromolecules are mainly negative during the nighttime cycle, and that a substantial fraction of the macromolecule population is in the neutral state during the daytime, when photoelectric ejection of electrons via UV radiation is possible. On the other hand, the aerosol population, depending on their size, becomes uniformly neutral or negatively charged during the night, but during the day, their dominant charge state is positive. Borucki et al. (2006), with a slightly more sophisticated model, find that the distributions of charge on the macromolecules show approximate agreement with those reported by Bakes et al. (2002).

These models of the lower atmosphere only considered three-body electron attachment to radicals or collisional charging of aerosols as a source of negatively charged species. Probably because the first process is negligible at high altitude (densities lower than 10^{15} cm^{-3}) and because aerosols were not expected to be present above $\sim 500 \text{ km}$, the possible presence of negative ions in Titan's upper atmosphere had not been considered before the Cassini–Huygens mission.

In this context, it came as a surprise when the Electron Spectrometer (ELS), one of the sensors making up the Cassini Plasma Spectrometer (CAPS), revealed the existence of numerous negative ions in Titan's upper atmosphere (Coates et al., 2007a; Waite et al., 2007). Waite et al. (2007) first reported a total negative ion density close to $10,000 \text{ cm}^{-3}$ but this incredibly high number was later corrected to $\sim 200 \text{ cm}^{-3}$ in Coates et al. (2007a), giving a total negative to positive ion ratio of ~ 0.1 . The spectrum (Fig. 3 in Coates et al. (2007a)) shows evidence for negatively charged ions up to $\sim 10,000 \text{ amu/q}$ as well as two distinct peaks at 12–20 and 28–45 amu/q . Negative ions have been detected on all Titan encounters when the spacecraft altitude was low enough and pointing conditions were favorable (Coates, 2009; Coates et al., 2007a, 2009).

These results have profound implications on our understanding of Titan's chemistry. Current photochemical models indicate that aerosol formation occurs through neutral chemistry in the stratosphere (Lebonnois et al., 2002; Wilson and Atreya, 2003) or around 800 km (Lavvas et al., 2008b). By analyzing the optical properties of the detached haze layer observed at 520 km in Titan's mesosphere, Lavvas et al. (2009) retrieved a mass flux of haze particles ($\sim 2 \times 10^{-14} \text{ g cm}^{-2} \text{ s}^{-1}$) approximately equal to the mass flux required to explain the main haze layer. This is the first quantitative evidence that thermospheric, instead of stratospheric chemistry, is the main source of haze on Titan and supports the results of Lavvas et al. (2008b).

However, the detection of nanometer size particles (1000 amu $\sim 1 \text{ nm}$), at an altitude as high as 1000 km, implies that molecular growth starts at even a higher altitude than this model predicts. The observation of a high density of charged molecules suggests that ion chemistry plays an important role in the formation of complex species. As a consequence, identifying the simplest negative ions observed by ELS as well as their production

pathways is crucial for our understanding of not only Titan's ionosphere but also the whole aerosol formation process.

In order to understand the presence of negative ions in Titan's thermosphere and investigate their larger role in chemical cycles on Titan, we present here an ionospheric chemistry model of formation of low mass negative ion species. We first describe the CAPS observations and data reduction in Section 2. Possible negative ion candidates are presented in Section 3 where production and destruction processes included in the model are reviewed. In Section 4 we discuss the parameters used in our model with most of the discussion centered on the supra-thermal electron flux and on the neutral atmosphere employed. Section 5 presents the model results and compares them with the observed negative ion mass spectrum. Section 6 discusses these results and Section 7 presents some concluding remarks.

2. CAPS-ELS observations

Cassini CAPS-ELS observations of Titan's ionosphere have revealed the existence of heavy negative ions at altitudes between ~ 1200 and 950 km with masses up to $\sim 10,000 \text{ amu/q}$ (Coates, 2009; Coates et al., 2007a, 2009; Waite et al., 2007). The ELS sensor is a hemispherical, electrostatic top-hat analyzer, which sweeps through a 63-point energy spectrum ranging from 0.6 to $28,000 \text{ eV/q}$ for negatively charged particles. The energy resolution, which corresponds to the energy bandwidth of the analyzer ($\Delta E/E$), is 16.7% (Young et al., 2004). The spectrometer has an instantaneous fan-shaped field of view of $160^\circ \times 5^\circ$, with each of the 8 anodes covering $20^\circ \times 5^\circ$ (Linder et al., 1998), thus providing directional information on the incident electrons. The CAPS instrument is mounted on a rotating platform called the actuator, which increases the angular coverage by rotating the instrument field of view around an axis parallel to the spacecraft z-axis. The maximum rotation is ± 104 degrees from the spacecraft $-Y$ direction, at a nominal rate of $1^\circ/\text{s}$.

The T40 flyby occurred on January 5, 2008 with a latitude, longitude and local time at closest approach of 12°S , 131°W and 14.3 h, respectively. Here, we focus on this flyby for two reasons: (i) the encounter occurred on the dayside with a solar zenith angle at closest approach (1015 km) of 37.5° . The main energy source upon Titan's upper atmosphere was solar photons, thus the induced supra-thermal electron intensities can be predicted theoretically, as presented in Section 4. (ii) Neutral, positive and negative ions as well as thermal electrons observations are available from INMS, CAPS-ELS and the Cassini Radio Plasma Wave Spectrometer Langmuir Probe (RPWS-LP).

The spacecraft potential becomes negative when the spacecraft passes through Titan's dense ionosphere where the ambient negative particle flux (mainly electrons) dominates the current balance to the spacecraft. The data is therefore shifted by a spacecraft potential of $-0.5 \pm 0.3 \text{ V}$ for T40. This value is based on comparing the INMS and CAPS-IBS (Ion Beam Spectrometer) ion data and requiring the peak positive ion flux to be at mass 28 (Crary et al., 2009). A key feature observed in Titan's supra-thermal spectra is the photoelectron peak at 24.1 eV associated with the ionization of N_2 by the strong He II (30.4 nm) solar line (see Section 4.1). Applying a spacecraft potential correction of -0.5 eV gives a photoelectron peak value of $22.7 \pm 1.9 \text{ V}$. The error is due to the ELS energy resolution of 16.7% and the spacecraft potential correction. This spacecraft potential value is therefore consistent with the theoretical prediction for the photoelectron peak location.

As the CAPS actuator moves the ELS field of view through the ram direction in Titan's ionosphere, distinct spikes in energy appear in the ELS spectrogram, as presented in Fig. 1. These spikes

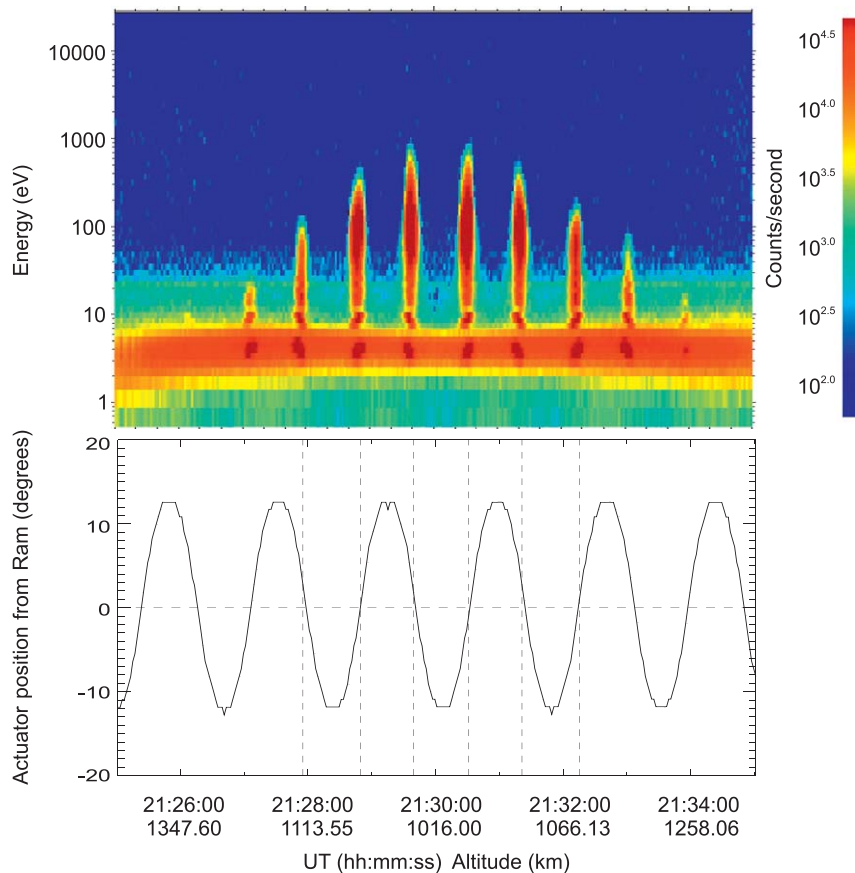


Fig. 1. Energy–time spectrogram retrieved by ELS and the corresponding actuator/ram angle during the T40 encounter. The vertical spikes systematically occur at a 0° angle between the actuator and ram and can consequently be attributed as negative ions.

are the signatures of negative ions rather than electrons because ions have thermal velocities that are small compared to the spacecraft velocity whereas electrons are more isotropic due to their supra-thermal velocities and thus are detected from any actuator position. Negative ions were detected for approximately ± 3.5 minutes around closest approach, corresponding to an upper altitude of 1250 km.

The spacecraft ram velocity separates the masses of the cold ions in detected energy per charge. The peak energy per charge, once corrected for the spacecraft potential, can then be converted to mass per charge knowing the spacecraft speed. For example, a 6 km s^{-1} flyby speed gives $m_{\text{amu}/q} = 5.32 E_{\text{eV}/q}$ (Coates et al., 2007a). It is assumed that ions are singly charged, which is probably reasonable for the lighter ions ($< 100 \text{ amu}$). However, this assumption may be questionable for high m/q , giving an even higher m in the aerosol range in those cases (Coates et al., 2007a; Waite et al., 2007).

As seen on the spectrogram in Fig. 2, two negative ion peaks centered at 22 ± 4 and $44 \pm 8 \text{ amu}/q$ are clearly identified. A third peak at $82 \pm 14 \text{ amu}/q$ may be present as well. Keeping in mind the finite energy width of the detector ($\Delta E/E = 16.7\%$), the peak width is consistent with the presence of a single ion species per peak, though the presence of multiple species cannot be rejected.

3. Chemistry

Various negative ions have been suggested as potential candidates for the low mass peaks observed by ELS (Coates

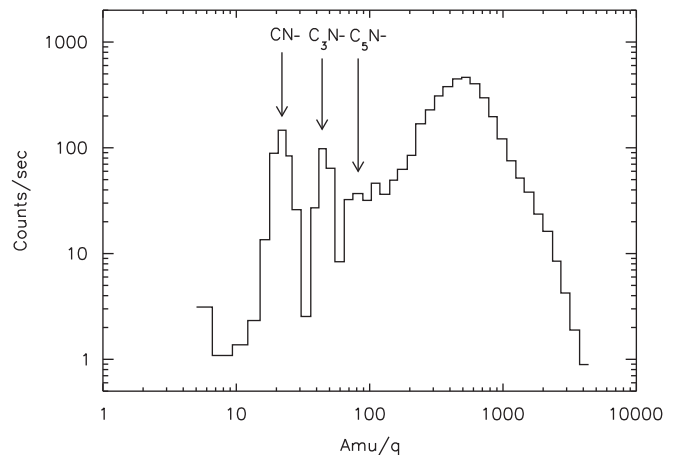


Fig. 2. Negative ions measured in each CAPS-ELS energy bin at an altitude of 1015 km during the T40 encounter. The attribution of the peaks is based on the ionospheric chemistry model.

et al., 2007a; Waite et al., 2007). In this section, we discuss the ions likely present in Titan's ionosphere based on their electron affinity and gas phase acidity (Table 1). Production mechanisms for negative ions include radiative and dissociative electron attachment and ion-pair formation, while loss processes are photodetachment, ion–ion recombination and ion–neutral associative detachment. Chemical reactions such as proton

Table 1
Electron affinity and gas phase acidity of some molecules present on Titan.

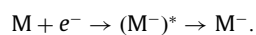
Species	Electron affinity (eV)	Refs.	Species	Acidity (kJ/mol)	Refs.
H	0.75	Hotop and Lineberger (1985)	H ₂	1649	Shiell et al. (2000)
<i>Hydrocarbons</i>					
CH ₂	0.65	Leopold et al. (1985)	CH ₄	1710	Ellison et al. (1978)
CH ₃	0.08	Ellison et al. (1978)			
<i>Polyynes</i>					
C ₂ H	3.0	Taylor et al. (1998)	C ₂ H ₂	1547	Ruscic and Berkowitz (1990)
C ₄ H	3.6	Taylor et al. (1998)	C ₄ H ₂	1474	Taylor et al. (1998)
C ₆ H	3.8	Taylor et al. (1998)	C ₆ H ₂	1467	Taylor et al. (1998)
C ₈ H	4.0	Taylor et al. (1998)	C ₈ H ₂	1451	Taylor et al. (1998)
<i>Aromatic hydrocarbons</i>					
C ₆ H ₅	1.1	Gunion et al. (1992)	C ₆ H ₆	1644	Davico et al. (1995)
CH ₂ C ₆ H ₅	0.9	Gunion et al. (1992)	CH ₃ C ₆ H ₅	1557	Gal et al. (2001)
<i>Nitriles</i>					
CN	3.8	Bradforth et al. (1993)	HCN	1438	Bradforth et al. (1993)
CH ₂ CN	1.5	Moran et al. (1987)	CH ₃ CN	1528	Bartmess et al. (1979)
C ₃ N	4.6	Graupner et al. (2006)	HC ₃ N	1435	Taft et al. (1988)
C ₅ N	4.5	Botschwina (1996)	HC ₅ N	–	–
<i>Non-saturated nitrogen-bearing species</i>					
NH ₂	0.8	Wickham-Jones et al. (1989)	NH ₃	1657	Wickham-Jones et al. (1989)
CH ₂ N	0.5	Cowles et al. (1991)	CH ₂ NH	1594	Kass and DePuy (1985)
<i>Oxygen-bearing species</i>					
O	1.5	Hotop and Lineberger (1985)	H ₂ O	1605	Schulz et al. (1982)
OH	1.8	Schulz et al. (1982)			

No data was found for the acidity of HC₅N.

transfer reactions and polymerization reactions can also influence the ion distribution. In the following, we review all these mechanisms in the context of Titan' ionosphere. Photochemical reactions and chemical reactions included in our model are listed in Tables 2 and 3, respectively.

3.1. Negative ion candidates

The stability of a negative ion can be characterized by the electron affinity (EA) of its parent molecule, which describes its efficiency towards electron attachment,



The larger the EA for molecule M, the more stable M[−] will be. Adding an electron to the filled valence shell of a molecule is difficult because the associated anion lies at a higher-energy than the neutral ground state and as a consequence the activated complex (M[−])^{*} has a very short lifetime against auto-detachment. For this reason, negative ions are expected to be mostly deprotonated neutrals and we do not consider closed-shell molecules such as C₂H₂[−] or HCN[−] to be plausible negative ion candidates.

Another relevant thermodynamic constant is the gas phase acidity of the molecule AH, which characterizes the ability of the molecule to lose a H⁺,



Table 1 provides a list of the EA of 16 different atoms and radicals and the gas phase acidity of 14 different molecules considered as potential sources of negative ions. The species included in Table 1 are based on observations, such as the positive ion mass spectra obtained by INMS (Vuitton et al., 2007).

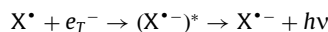
We can see in Table 1 that species containing the cyano (CN, C₃N) or the ethynyl (C₂H, C₄H, C₆H, C₈H) group have a very high EA (≥3 eV). Oxygen-bearing species (O, OH) have a moderately high EA (~1.5 eV) and acidity, while other hydrocarbons and non-

saturated nitrogen-bearing species have a somewhat low EA (≤1.0 eV) and moderate acidity. HCN, HC₃N and the polyne family are strong acids, while H₂O, aromatic hydrocarbons and other nitrogen-bearing species are moderately acidic. Finally, H₂ and CH₄ are very weak acids. Based on these considerations, we selected 19 neutrals and 11 anions to be included in our ionospheric chemistry model: O[−], OH[−], CH₃[−], C₂H[−], C₄H[−], C₆H[−], CN[−], C₃N[−] and C₅N[−]. Despite the fact that H and CH₂ have a low EA (≤0.75 eV), H[−] and CH₂[−] are readily formed by electron attachment to CH₄ (see Section 3.2.1) and because of the high mole fraction of CH₄ in Titan's atmosphere, we consider these ions as well in the model.

3.2. Sources of negative ions

3.2.1. Radiative electron attachment

Radiative attachment of thermal electrons to atoms or radicals is a process that can lead to the formation of negative ions,



As mentioned previously, attachment to stable molecules is of negligible efficiency because the resulting anion is unstable with respect to auto-detachment. In the following, we consider radiative attachment to radicals predicted to be abundant in Titan's thermosphere by photochemical models. Table 2 contains some relevant attachment rate coefficients.

Electron attachment reactions to C₂H, C₄H, C₆H and C₃N lead to the formation of negative ions, C₂H[−], C₄H[−], C₆H[−] and C₃N[−], respectively. The radiative attachment to these species has not been studied experimentally. Herbst and Osamura (2008) used phase-state theory in order to calculate the rate coefficients of these reactions. As expected, the attachment efficiency increases with the size of the molecule, from a tiny value for C₂H ($2 \times 10^{-15}(T_e/300)^{-0.5} \text{ cm}^3 \text{ s}^{-1}$) to the collisional rate for C₆H radicals ($3 \times 10^{-10}(T_e/300)^{-0.5} \text{ cm}^3 \text{ s}^{-1}$).

Table 2
Reaction list: photochemical reactions.

# Reaction	Cross section/reaction rate	Refs.
<i>Ion-pair formation</i>		
$H_2+h\nu \rightarrow H^-+H^+$	2.5×10^{-23} @ 17.3	Berkowitz (1996), Chupka et al. (1975)
$CH_4+h\nu \rightarrow H^-+CH_3^+$	1.0×10^{-20} @ 21.5	Berkowitz (1996), Mitsuke et al. (1991)
$C_2H_2+h\nu \rightarrow C_2H^-+H^+$	6.0×10^{-21} @ 18.8	Berkowitz (1996), Ruscic and Berkowitz (1990)
$HCN+h\nu \rightarrow CN^-+H^+$	4.4×10^{-20} @ 15.2	Berkowitz (1996), Berkowitz et al. (1969)
$CO+h\nu \rightarrow O^-+C^+$	1.1×10^{-19} @ 20.9	Berkowitz (1996), Oertel et al. (1980)
$H_2O+h\nu \rightarrow OH^-+O^+$	1.1×10^{-20} @ 16.9	Berkowitz (1996)
<i>Dissociative electron attachment</i>		
$CH_4+e_{5^-} \rightarrow CH_2^-+H_2$	9.5×10^{-20} @ 10.3	Sharp and Dowell (1967)
$\rightarrow H^-+CH_3$	7.2×10^{-20} @ 8.9	
$C_2H_2+e_{5^-} \rightarrow C_2H^-+H$	7.0×10^{-20} @ 2.7, 7.7	Rutkowski et al. (1980)
$C_4H_2+e_{5^-} \rightarrow C_4H^-+H$		Est. from C_2H_2
$C_6H_2+e_{5^-} \rightarrow C_6H^-+H$		Est. from C_2H_2
$HCN+e_{5^-} \rightarrow CN^-+H$	2.0×10^{-16} @ 2.5	Inoue (1966)
$CH_3CN+e_{5^-} \rightarrow CN^-+CH_3$	4.2×10^{-25} @ 2.0	
	1.1×10^{-24} @ 8.0	Sailer et al. (2003)
$C_2H_3CN+e_{5^-} \rightarrow CN^-+C_2H_3$		Tsuda et al. (1973)
$HC_3N+e_{5^-} \rightarrow CN^-+C_2H$	4.0×10^{-18} @ 4.9	Dibeler et al. (1961)
$\rightarrow C_3N^-+H$	3.8×10^{-18} @ 2.6	See text
$HC_5N+e_{5^-} \rightarrow CN^-+C_2H$		Est. from HC_3N
$\rightarrow C_5N^-+H$		Est. from HC_3N
$C_2N_2+e_{5^-} \rightarrow CN^-+CN$	1.9×10^{-17} @ 5.5	Inoue (1966)
$CO+e_{5^-} \rightarrow O^-+C$	2.0×10^{-19} @ 9.8	Rapp and Briglia (1965), Stamatovic and Schulz (1970)
$H_2O+e_{5^-} \rightarrow H^-+OH$	5.5×10^{-18} @ 6.6	Haxton et al. (2007)
$\rightarrow O^-+H_2$	9.0×10^{-19} @ 12.	
$\rightarrow OH^-+H$	4.9×10^{-20} @ 7.0	Fedor and Cicman et al. (2006)
<i>Radiative electron attachment</i>		
$H+e_{7^-} \rightarrow H^-+h\nu$	$3.0 \times 10^{-16}(T_e/300)$	Ohio State University Database (2007) ^a
$CH_2+e_{7^-} \rightarrow CH_3^-+h\nu$		Est. from CN
$CH_3+e_{7^-} \rightarrow CH_3^-+h\nu$		Est. from CN
$C_2H+e_{7^-} \rightarrow C_2H^-+h\nu$	$2.0 \times 10^{-15}(T_e/300)^{-0.5}$	Herbst and Osamura (2008)
$C_4H+e_{7^-} \rightarrow C_4H^-+h\nu$	$1.1 \times 10^{-8}(T_e/300)^{-0.5}$	Herbst and Osamura (2008)
$C_6H+e_{7^-} \rightarrow C_6H^-+h\nu$	$6.2 \times 10^{-8}(T_e/300)^{-0.5}$	Herbst and Osamura (2008)
$CN+e_{7^-} \rightarrow CN^-+h\nu$	1.0×10^{-14}	Petrie (1996)
$C_3N+e_{7^-} \rightarrow C_3N^-+h\nu$	$2.6 \times 10^{-10}(T_e/300)^{-0.5}$	Herbst and Osamura (2008)
$C_5N+e_{7^-} \rightarrow C_5N^-+h\nu$		Est. from C_6H
$O+e_{7^-} \rightarrow O^-+h\nu$	1.5×10^{-15}	Ohio State University Database (2007) ^a
$OH+e_{7^-} \rightarrow OH^-+h\nu$		Est. from CN

For ion-pair formation and dissociative electron attachment reactions, the maximum of the cross section (cm^2) and its location (eV) are given. For radiative electron attachment, the rate constant ($cm^3 s^{-1}$) is given. e_{5^-} and e_{7^-} stand for supra-thermal and thermal electrons, respectively.

^a <http://www.physics.ohio-state.edu/~eric/research.html>.

The H^- , CH_2^- , CH_3^- , OH^- and CN^- anions can be produced by thermal electron capture by the neutral molecules but the rate coefficients have not been determined. These are small species and thus have few rotational and vibrational degrees of freedom available for energy dispersal. As a consequence, radiative attachment is likely to proceed at a rate only slightly faster than that of an atomic species. We adopt a rate constant of $10^{-14} cm^3 s^{-1}$, as suggested by Petrie (1996) in his study of CN^- formation pathways in interstellar clouds and circumstellar envelopes.

Table 3
Reaction list: chemical reactions.

# Reaction	Rate constant	Refs.
$H^-+X^+ \rightarrow Products$	1.0×10^{-7}	Hickman (1979), Smith et al. (1978)
$H^-+R \rightarrow Products+e_{7^-}$	1.8×10^{-9}	Fehsenfeld et al. (1973)
$H^-+C_2H_2 \rightarrow C_2H^-+H_2$	4.4×10^{-9}	Mackay et al. (1977)
$H^-+C_4H_2 \rightarrow C_4H^-+H_2$	6.4×10^{-9}	k_L
$H^-+C_6H_2 \rightarrow C_6H^-+H_2$	6.3×10^{-9}	k_L
$H^-+HCN \rightarrow CN^-+H_2$	1.5×10^{-8}	Mackay et al. (1976)
$H^-+HC_3N \rightarrow C_3N^-+H_2$	1.0×10^{-8}	k_L
$H^-+HC_5N \rightarrow C_5N^-+H_2$	1.0×10^{-8}	k_L
$CH_2^-+X^+ \rightarrow Products$	1.0×10^{-7}	Hickman (1979), Smith et al. (1978)
$CH_2^-+R \rightarrow Products+e_{7^-}$	1.0×10^{-9}	Adams (1996)
$CH_3^-+X^+ \rightarrow Products$	1.0×10^{-7}	Hickman (1979), Smith et al. (1978)
$CH_3^-+R \rightarrow Products+e_{7^-}$	1.0×10^{-9}	Adams (1996)
$C_2H^-+X^+ \rightarrow Products$	1.0×10^{-7}	Hickman (1979), Smith et al. (1978)
$C_2H^-+R \rightarrow Products+e_{7^-}$	1.6×10^{-9}	Barckholtz et al. (2001)
$C_2H^-+C_4H_2 \rightarrow C_4H^-+C_2H_2$	1.5×10^{-9}	k_L
$C_2H^-+C_6H_2 \rightarrow C_6H^-+C_2H_2$	2.3×10^{-9}	k_L
$C_2H^-+HCN \rightarrow CN^-+C_2H_2$	3.9×10^{-9}	Mackay et al. (1976)
$C_2H^-+HC_3N \rightarrow C_3N^-+C_2H_2$	2.5×10^{-9}	k_L
$C_2H^-+HC_5N \rightarrow C_5N^-+C_2H_2$	2.9×10^{-9}	k_L
$C_2H^-+C_2H_2 \rightarrow C_4H^-+H_2$	1.0×10^{-12}	De Bleecker et al. (2006), Howling et al. (1994)
$C_4H^-+X^+ \rightarrow Products$	1.0×10^{-7}	Hickman (1979), Smith et al. (1978)
$C_4H^-+R \rightarrow Products+e_{7^-}$	8.3×10^{-10}	Barckholtz et al. (2001)
$C_4H^-+C_6H_2 \rightarrow C_6H^-+C_2H_2$	1.8×10^{-9}	k_L
$C_4H^-+HCN \rightarrow CN^-+C_2H_2$	2.0×10^{-9}	k_L
$C_4H^-+HC_3N \rightarrow C_3N^-+C_2H_2$	2.0×10^{-9}	k_L
$C_4H^-+HC_5N \rightarrow C_5N^-+C_2H_2$	2.3×10^{-9}	k_L
$C_4H^-+C_2H_2 \rightarrow C_6H^-+H_2$	1.0×10^{-12}	De Bleecker et al. (2006), Howling et al. (1994)
$C_6H^-+X^+ \rightarrow Products$	1.0×10^{-7}	Hickman (1979); Smith et al. (1978)
$C_6H^-+R \rightarrow Products+e_{7^-}$	5.0×10^{-10}	Barckholtz et al. (2001)
$C_6H^-+HCN \rightarrow CN^-+C_2H_2$	1.9×10^{-9}	k_L
$C_6H^-+HC_3N \rightarrow C_3N^-+C_2H_2$	1.8×10^{-9}	k_L
$C_6H^-+HC_5N \rightarrow C_5N^-+C_2H_2$	2.1×10^{-9}	k_L
$C_6H^-+C_2H_2 \rightarrow C_xH_yN_z$	1.0×10^{-12}	De Bleecker et al. (2006), Howling et al. (1994)
$CN^-+X^+ \rightarrow Products$	1.0×10^{-7}	Hickman (1979), Smith et al. (1978)
$CN^-+R \rightarrow Products+e_{7^-}$	1.3×10^{-9}	Fehsenfeld (1975)
$CN^-+HC_3N \rightarrow C_3N^-+HCN$	4.6×10^{-9}	k_L
$CN^-+HC_5N \rightarrow C_5N^-+HCN$	5.4×10^{-9}	k_L
$C_3N^-+X^+ \rightarrow Products$	1.0×10^{-7}	Hickman (1979), Smith et al. (1978)
$C_3N^-+R \rightarrow Products+e_{7^-}$	1.0×10^{-9}	Petrie and Herbst (1997)
$C_5N^-+X^+ \rightarrow Products$	1.0×10^{-7}	Hickman (1979), Smith et al. (1978)
$C_5N^-+R \rightarrow Products+e_{7^-}$		Est. from C_3N^-
$O^-+X^+ \rightarrow Products$	1.0×10^{-7}	Hickman (1979), Smith et al. (1978)
$O^-+R \rightarrow Products+e_{7^-}$	5.0×10^{-10}	UMIST Database (2005) ^a
$O^-+CH_4 \rightarrow OH^-+CH_3$	1.0×10^{-10}	Bohme and Fehsenfeld (1969)
$O^-+C_2H_2 \rightarrow Products+e_{7^-}$	$1.1 \times 10^{-9} (300/T)^{0.39}$	Viggiano and Paulson (1983)
$O^-+C_2H_2 \rightarrow C_2H^-+OH$	$1.8 \times 10^{-9} e^{-289/T}$	Viggiano and Paulson (1983)
$O^-+C_4H_2 \rightarrow C_4H^-+OH$	1.6×10^{-9}	k_L

Table 3 (continued)

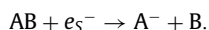
# Reaction	Rate constant	Refs.
$O^- + C_6H_2 \rightarrow C_6H^- + OH$	1.6×10^{-9}	k_L
$O^- + HCN \rightarrow CN^- + OH$	3.7×10^{-9}	Bohme (1975)
$O^- + HC_3N \rightarrow C_3N^- + OH$	2.9×10^{-9}	k_L
$O^- + HC_5N \rightarrow C_5N^- + OH$	2.8×10^{-9}	k_L
$OH^- + X^+ \rightarrow \text{Products}$	1.0×10^{-7}	Hickman (1979), Smith et al. (1978)
$OH^- + R \rightarrow H_2O + e_T^-$	1.4×10^{-9}	Howard et al. (1974)
$OH^- + C_2H_2 \rightarrow C_2H^- + H_2O$	2.2×10^{-9}	Raksit and Bohme (1983)
$OH^- + HCN \rightarrow CN^- + H_2O$	3.5×10^{-9}	Raksit and Bohme (1983)
$C_xH_yN_z + X^+ \rightarrow \text{Products}$	1.0×10^{-7}	Hickman (1979), Smith et al. (1978)
$C_xH_yN_z + R \rightarrow \text{Products} + e_T^-$	1.0×10^{-9}	Adams (1996)

Rate constants are given in $\text{cm}^3 \text{s}^{-1}$.

^a <http://www.udfa.net/>.

3.2.2. Dissociative electron attachment

Dissociative attachment is endothermic for most species because the energy of the bond broken exceeds the electron affinity. For example, the H–C bond energy in acetylene is 5.7 eV (Ervin et al., 1990), greater than the electron affinity of C_2H (3.0 eV). As a consequence, dissociative attachment reactions require supra-thermal electrons that can overcome the energy difference,



The CN^- anion can be produced by dissociative electron capture on various nitrile species. The presence of HCN, C_2N_2 , CH_3CN , C_2H_3CN and HC_3N has been inferred from analysis of INMS spectra with mixing ratios ranging from 2×10^{-4} to 2×10^{-6} as detailed in Section 4.2 (Cui et al., 2009; Vuitton et al., 2007). Inoue (1966) performed a systematic study on the formation of negative ions in hydrogen cyanide and cyanogen. They estimated the cross section for electron attachment on HCN and C_2N_2 at the maximum of the resonance peak to be $2 \times 10^{-16} \text{ cm}^2$ (at 2.5 eV) and $2 \times 10^{-17} \text{ cm}^2$ (at 5.3 eV), respectively. Sailer et al. (2003) reported low energy electron attachment cross sections for acetonitrile (CH_3CN) in the energy range from about 0.1 up to 10 eV. The cross section for formation of CN^- is small with peak values of $\sim 4 \times 10^{-21} \text{ cm}^2$ at 1.8 eV and $\sim 10^{-20} \text{ cm}^2$ at 9.2 eV. For acrylonitrile (C_2H_3CN), the CN^- yield curve exhibits 3 peaks at ~ 2 , ~ 3 and ~ 6 eV (Heni and Illenberger, 1986; Tsuda et al., 1973). Comparison of the yield of CN^- ions with that of $C_2H_3CN^+$ gave the value 47.6 for $C_2H_3CN^+/CN^-$ at 9.5 eV (15 eV for the positive ions) (Tsuda et al., 1973). The total impact cross section of C_2H_3CN is unknown and we have estimated it to be equal to that of C_4H_2 (Kim and Irikura, 2000).

The supra-thermal electron impact on HC_3N has two possible product channels regarding negative ion formation: (C_3N^- , H) and (CN^- , C_2H). Dibeler et al. (1961) provide information about the magnitude at the peak of the resonance profiles relative to the total electron impact cross section of HC_3N at 70 eV, with values of 0.02 and 0.018 for each channel, respectively. In the absence of any further information for this molecule, we have assumed a Gaussian profile for the cross section of each pathway with a FWHM of ~ 1 eV, which is in the order of typical widths found in all other measured resonance profiles of negative ion production induced by electron impact. The location of the peak for each profile was derived from the assumed width of the distribution and the observed apparition energy for each pathway, 3.5 eV for C_3N^- and 6.0 eV for CN^- . The total impact cross section of HC_3N is also unknown and we have estimated it to be equal to that of C_4H_2 (Kim and Irikura, 2000).

The C_2H^- anion is produced by dissociative attachment on C_2H_2 . Rutkowski et al. (1980) investigated the negative ion formation of a few simple hydrocarbons in the energy range 0.1–15 eV and measured the cross section for the dissociative attachment to C_2H_2 . Two separate peaks with a sharp resonant-like behavior can be distinguished around 3 and 8 eV with a maximum of $\sim 7 \times 10^{-20} \text{ cm}^2$. Two overlapping, unresolved peaks are present in the dissociative attachment in methane. The lower-energy peak at ~ 9 eV is due to H^- and the higher-energy peak at ~ 10 eV to CH_2^- . The maximum cross section is close to 10^{-19} cm^2 (Sharp and Dowell, 1967).

The absolute total cross sections for O^- formation from CO by electron impact has been measured by Rapp and Briglia (1965) to be $2 \times 10^{-19} \text{ cm}^2$ at its peak (9.9 eV). Using this value, Stamatovic and Schulz (1970) determined that the maximum cross section for C^- formation is about $6 \times 10^{-23} \text{ cm}^2$ at 10.4 eV. Because of the small magnitude of the cross section, we do not consider the formation of C^- in our model. Ion yields for the formation of the three fragments H^- , O^- and OH^- as a result of dissociative attachment to water were measured as a function of the incident electron energy by Fedor et al. (2006). The experimental data, which do not have absolute normalization, are normalized to agree with the Compton and Christophorou (1967) $H^- + OH$ peak height for the lowest energy resonance at $6.5 \times 10^{-18} \text{ cm}^2$. Cross sections for dissociative electron attachment are presented in Fig. 3.

3.2.3. Ion-pair formation

In some cases, photo-ionization can induce the formation of a positive ion/negative ion pair,



The cross section for ion-pair production is usually 10^2 – 10^5 times smaller than that for the formation of a positive ion and a neutral. In the model, ionization of CH_4 and H_2 produces H^- (Chupka et al., 1975; Mitsuke et al., 1991). We also include ionization of C_2H_2 and HCN as a source of C_2H^- and CN^- , respectively (Berkowitz et al., 1969; Ruscic and Berkowitz, 1990). Finally, CO and H_2O produce O^- and OH^- , respectively (Berkowitz 1996; Oertel et al., 1980). Thresholds and cross sections for these processes are listed in Table 2.

3.3. Losses for negative ions

3.3.1. Photo-detachment

For the photo-detachment rates, we have assumed the cross section σ to depend on photon energy ε via the relation

$$\sigma = \sigma_0(1 - EA/\varepsilon)^{0.5}, \quad \varepsilon \geq EA,$$

where $\sigma_0 = 10^{-17} \text{ cm}^2$ and EA is the electron affinity of the neutral molecule (Millar et al., 2007). Relevant electron affinities have been obtained from theoretical and experimental results, and are shown in Table 1.

3.3.2. Ion-ion recombination

Not much information is available on this process. A complex potential model has been used to treat the mutual neutralization of positive and negative ions (Hickman, 1979). The numerical results of the theory have been parameterized in terms of the reduced mass of the collision and the electron affinity of the electron donor,

$$k = 5.34 \times 10^{-7} EA^{-0.4} m_{ij}^{-0.5} (T_{\text{gas}}/300)^{-0.5} \text{ cm}^3 \text{ s}^{-1}$$

This is consistent with experimental results, rate constants varying from about 5×10^{-8} to $10^{-7} \text{ cm}^3 \text{ s}^{-1}$ at room temperature

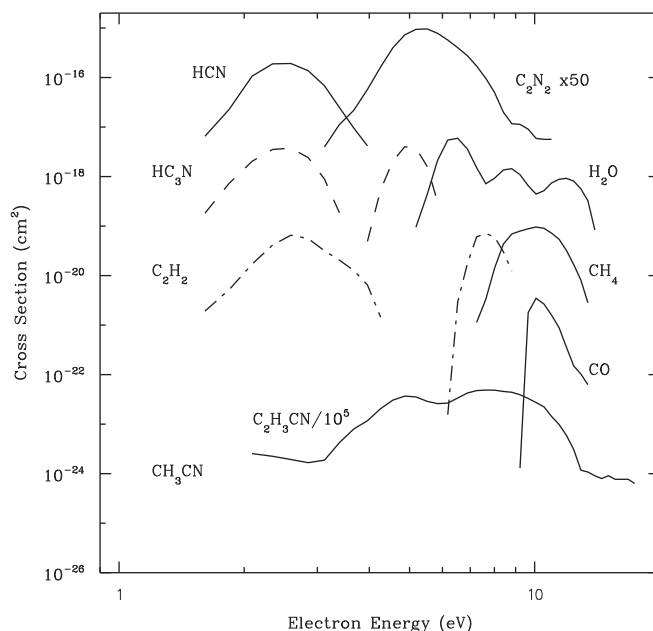


Fig. 3. Electron attachment cross-sections considered in the ionospheric chemistry model. References can be found in Table 2.

with power law temperature dependencies of ~ 0.5 for both simple and cluster ion reactions (Smith et al., 1978).

3.3.3. Ion–neutral associative detachment

In associative detachment, the negative ion attaches to the neutral, and the metastable species thus produced is stabilized by the ejection of the electron,



Such reactions can only occur when the electron detachment energy is less than the energy of the bond that is produced. Therefore, these reactions usually involve radical species that produce stable molecules. In the model, we consider the reaction of the negative ions with the two most abundant radicals in Titan's upper atmosphere, H and CH₃. The rate constants for reaction with H are usually an appreciable fraction of the collisional value (see Table 3). For reaction with CH₃, no data was found in the literature and we adopted the same rate constants as for reaction with H.

Viggiano and Paulson (1983) measured the temperature dependences of the rate coefficients for the associative detachment reactions O⁻+NO, S⁻+CO, S⁻+O₂, O⁻+C₂H₂ and O⁻+C₂H₄. The first three rate coefficients varied as $T^{-0.74 \pm 0.1}$, while the last two exhibited more complicated temperature dependences. Because of the lack of data for the reactions of interest here, we did not consider any temperature dependence for associative detachment reactions in the model.

3.4. Chemical reactions

3.4.1. Proton transfer reactions

Since we consider singly charged anions (A⁻) of acids AH, the most obvious chemical reaction is proton abstraction from HA by a strong base B⁻,

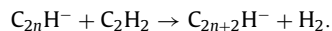
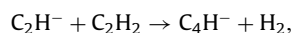


In Table 1 a list of the gas phase acidities of the molecules included in the ionospheric chemistry model is given. Methane and molecular hydrogen are the least acidic of all molecules, and the methyl and hydrogen anions will readily abstract a proton

from other neutral species. Exothermic proton transfers are almost always extremely fast in the gas phase, generally occurring at every collision. Therefore we adopt a rate constant equal to the Langevin rate for all reactions that have not been studied (Lequeux, 2005).

3.4.2. Polymerization reactions

Incorporation of anions in neutral molecules can lead to higher mass anions. According to the spectral pattern of the mass spectrum of the negative ions in an acetylene discharge, the repeated insertion of acetylene molecules results in an anion sequence with anions that peaks at the C_{2n}H⁻ species (Deschenaux et al., 1999). Therefore, C₂H⁻ anions can trigger a consecutive chain of polymerization reactions that evolves as follows:



So far no precise rate coefficients for these anion chain reactions can be found in the literature. Based on ions growth rate in silane discharges (Howling et al., 1994; Perrin et al., 1994), the rate coefficient for these reactions is set to $10^{-12} \text{ cm}^3 \text{ s}^{-1}$.

4. Model calculations

In order to investigate how the above processes define the formation of negative ions in Titan's atmosphere we extend the ionospheric chemistry model described in Vuitton et al. (2007). This model was successfully used for the investigation of the processes controlling the positive ion formation in Titan's ionosphere at the abundances observed by the INMS measurements. Furthermore, it was used for the investigation of the ion–neutral chemical processes controlling the formation of the observed thermospheric benzene abundance (Vuitton et al., 2008).

The ionospheric chemistry model solves the continuity equation in one-dimension assuming local chemical equilibrium. It takes into account production and loss processes that include photo-ionization, photo-detachment, energetic electron impact,

and chemical reactions between ions and ion–neutral species in the altitude range between 700 and 1200 km. Due to the small chemical lifetime of ions compared with the characteristic time for diffusion at these altitudes, the latter is not included in the calculations. Here, we will only describe the ionization mechanisms that lead to the production of negative ions, and the background atmospheric conditions assumed in the calculations regarding the neutral species abundances. Yet, the model includes the complete formation of positive ions as well, the details of which along with a complete description of the model can be found in Vuitton et al. (2007).

4.1. Ionization mechanisms

The solar flux used in the calculations is the measured flux by the TIMED/SEE instrument during the T40 flyby, scaled to Saturn's location (Woods, 2008; Woods et al., 2005). The daily average level 3 data product was used, which provides the solar flux on a 1-nm interval over the 0.5–194.5 nm range [http://lasp.colorado.edu/see/]. The solar zenith angle for T40 flyby is 37.5° at closest approach. The contribution of magnetospheric electrons as ionization source has been neglected since the latter is much smaller than the solar component over the illuminated side of Titan (Galand et al., 2006).

During the production of positive ions from the photoionization of neutral species, supra-thermal electrons are also produced. The energy of these photoelectrons depends on the energy difference between the ionizing photon energy and the energy required to ionize the neutral species. After their formation, photoelectrons lose energy through collisions with neutral species, which can lead to the production of secondary electrons. In order to realistically estimate the production of negative ions due to electron impact on neutral species, the flux of energetic electrons at all possible energies must be known. This can be calculated by solving the Boltzmann kinetic equation assuming stationarity, which provides the intensity (elctr cm⁻² s⁻¹ eV⁻¹) of electrons at different energies, pitch angles and altitudes within the atmosphere (Galand et al., 1999 and references therein).

Here we solve a simplified version of the kinetic equation by integrating in all angles in order to calculate the mean intensity at each altitude and by assuming that the local flux of electrons is constant (which is equivalent to assuming that transport of the electrons is not important). Comparison with a model solving the full transport Boltzmann equation (Galand et al., 2006) shows that this approximation is valid up to 1200 km. Under these conditions the mean intensity of electrons at energy, $\bar{I}(z, E)$, can be described as

$$0 = S_{\odot}(z, E) + n_e(z) \frac{\partial [L(E)\bar{I}(z, E)]}{\partial E} + \sum_{k,pr} n_k(z) \sigma_k^T(E) \int_E^{E_{\max}} dE' R_{k,pr}(E, E') \bar{I}(z, E') - \sum_k n_k(z) \sigma_k^T(E) \bar{I}(z, E)$$

with $R_{k,pr}$ the redistribution function associated with the neutral k through the process, pr . The first term on the right-hand side of the equation is the angle-integrated production of photoelectrons at energy E . The second term describes the energy transfer from supra-thermal to thermal electrons through Coulomb collisions. The third term describes the degradation of higher-energy electrons to energy E through collisions with neutral species, along with the production of secondary electrons with energy E through the ionization of the neutrals by higher-energy electrons, and the last term is the loss of energy E electrons due to collisions

with neutral species, with $n_k(z)$ the density of neutral species k at altitude z and $\sigma_k^T(E)$ the total electron impact cross section between an electron of energy E and a neutral species k .

We solve the above kinetic equation on an energy grid of 200 bins ranging from 0.1 to 10⁴ eV, with exponentially increasing bin width. Based on the above description, the electron mean intensity at each energy depends on that of higher energies. Hence, under the finite description of the energy grid, the mean intensity can be calculated at each energy starting at the highest energy bin and working downwards.

The resulting electron flux at 1015 km is presented in Fig. 4. A key feature is the peak at 24.1 eV associated with the ionization of N₂ by the strong He II (30.4 nm) solar line while the minimum in the region between 1 and 5 eV is due to the vibrational excitation of N₂ (e.g., Cravens et al., 2004; Galand et al., 2006, Coates et al., 2007b).

4.2. Abundance of neutral constituents

The ionospheric chemistry model requires density profiles for the neutral species. Furthermore, due to the large abundance of some radicals that have a high electron affinity, their inclusion in the calculations is necessary since they can also participate in the production of negative ions, as for example, C₃N. The neutral species included in the kinetic model are listed in Table 4. We base our vertical profiles on the INMS observations and the Lavvas et al. (2008b) photochemical model. The profiles presented in Vuitton et al. (2008) for the hydrocarbons and Hörst et al. (2008) for the O-bearing species are in good agreement with the results of Lavvas et al. (2008b).

Fig. 5 shows INMS measurements of the ion composition obtained during the T40 pass. The spectrum represents the average composition in the 1015–1050 km region of the atmosphere, obtained near the time of closest approach. Error bars shown in the figure represent the uncertainty due to counting statistics. Identification of the ions is discussed in Vuitton et al. (2007). The solar zenith angle was 37.5°, so the encounter was squarely in the sunlit atmosphere. The large ion

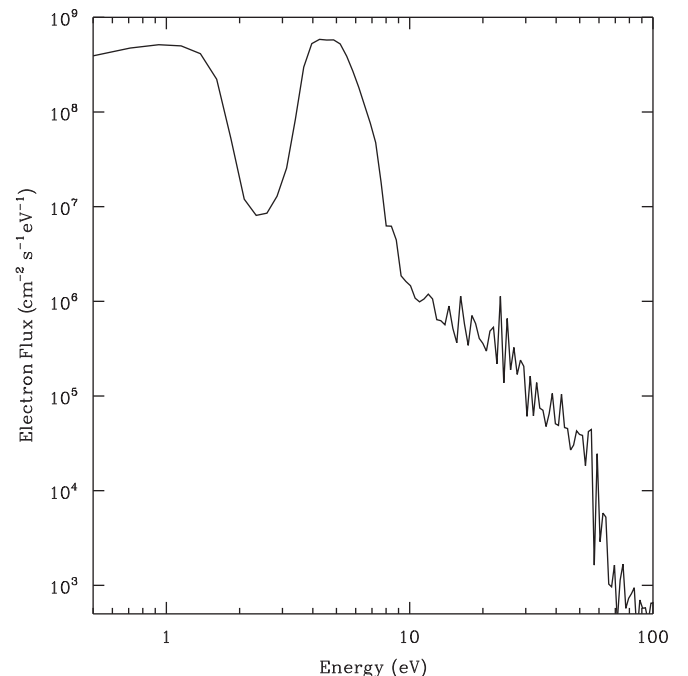


Fig. 4. Calculated energetic electrons flux at 1015 km.

Table 4
Mole fraction at 1015 km of the neutral species considered in the ionospheric chemistry model.

Species	Mole fraction
<i>Hydrocarbons</i>	
H ^a	9.9×10^{-4}
H ₂ ^b	3.8×10^{-3}
CH ₃ ^a	2.7×10^{-4}
CH ₄ ^b	2.8×10^{-2}
C ₂ H ^a	2.3×10^{-8}
C ₂ H ₂ ^a	9.9×10^{-4}
C ₄ H ^c	9.3×10^{-10}
C ₄ H ₂ ^d	1.1×10^{-5}
C ₆ H ^c	3.5×10^{-11}
C ₆ H ₂ ^d	1.1×10^{-6}
<i>Nitrogen-bearing species</i>	
N ₂ ^b	9.6×10^{-1}
C ₂ N ₂ ^a	9.3×10^{-6}
CN ^c	7.1×10^{-9}
HCN ^d	1.9×10^{-4}
CH ₃ CN ^d	9.9×10^{-7}
C ₂ H ₃ CN ^d	2.2×10^{-6}
C ₃ N ^c	2.0×10^{-8}
HC ₃ N ^d	3.4×10^{-5}
HC ₅ N ^d	1.3×10^{-6}
<i>Oxygen-bearing species</i>	
H ₂ O ^e	2.6×10^{-7}
CO ^e	9.8×10^{-6}

^a Photochemical model of Lavvas et al. (2008b).

^b INMS neutral measurements obtained on the Cassini T40 flyby.

^c Photochemical model of Lavvas et al. (2008b) scaled to the observed density of the parent molecule (see text).

^d Inferred from INMS ion measurements obtained on the Cassini T40 flyby (see text).

^e Unpublished results from the photochemical model of Lavvas et al. (2008a, b)

densities compared with, for example, the twilight T5 pass (Vuitton et al., 2007), supports earlier conclusions that solar energy deposition dominates over magnetospheric energy deposition in the sunlit atmosphere (Galand et al., 2006).

The N₂, H₂ and CH₄ densities are inferred from the T40 INMS neutral data. The densities at 1015 km of HCN, CH₃CN, HC₃N, C₂H₃CN, HC₅N, C₄H₂ and C₆H₂ are tuned for the ionospheric chemistry model to produce agreement with the observed densities of their associated protonated species for the T40 flyby, as explained in Vuitton et al. (2007). For these species, the vertical profiles from the Lavvas et al. (2008b) photochemical model are scaled to the mole fractions thus retrieved at 1015 km. For the radical species (CN, C₃N, C₅N, C₂H, C₄H, C₆H), the abundances calculated by the model of Lavvas et al. (2008b) are scaled with the correction factor of their corresponding closed-shell species (HCN, HC₃N, C₂H₂, C₄H₂, C₆H₂). Finally, for H, CH₃, C₂N₂, H₂O and CO, we did not apply any correction to the model results of Lavvas et al. (2008b). The mole fractions of some important molecules and radicals are presented in Fig. 6. The corresponding mole fractions at 1015 km are gathered in Table 4.

Fig. 5 (dotted line) shows the positive ion densities calculated with the neutral densities presented on Fig. 6. The relatively good fit indicates that the neutral composition is approximately correct. The main peaks at 28, 52, 76 and 51, 75 amu define the densities of HCN, HC₃N, HC₅N and C₄H₂, C₆H₂, respectively. Further details for the ion-chemical processes involved in the simulation of the positive ions chemistry can be found in Vuitton et al. (2007).

5. Results

The densities of the 11 negative ion species inferred from these neutral densities, the supra-thermal electron intensity and our

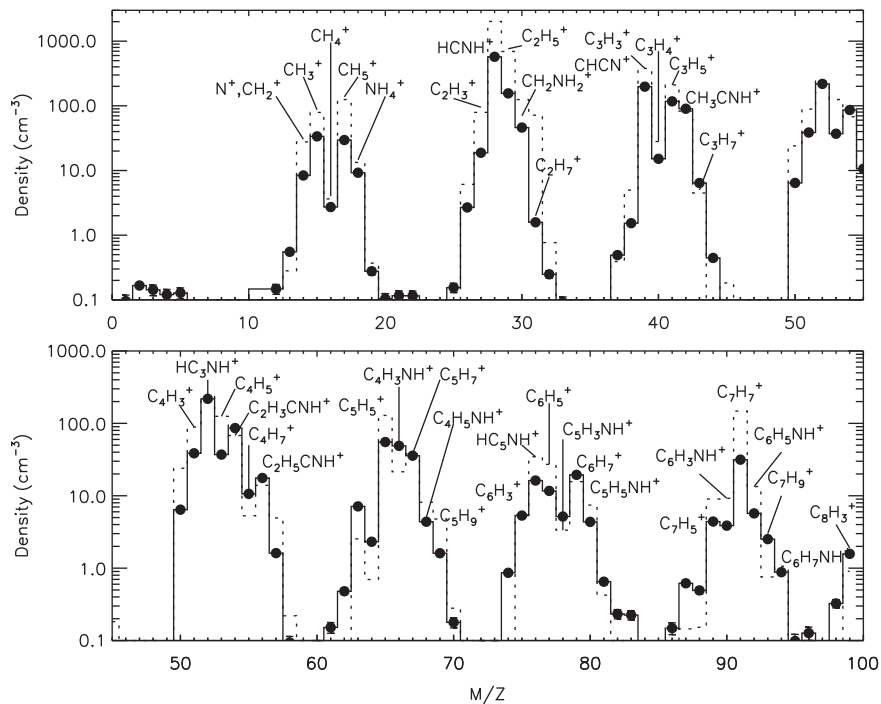


Fig. 5. Positive ions mass spectrum measured during the T40 encounter, averaged between the altitudes of 1015 and 1050 km and including both ingress and egress data. The black dots show the INMS measurements, and the black line connects the points. Error bars represent the uncertainty due to counting statistics. They are smaller than the symbol size for larger densities. They do not include a systematic error of 20% due to calibration uncertainties. The dotted line represents the modeled spectrum with densities of selected neutrals tuned to reproduce the observations.

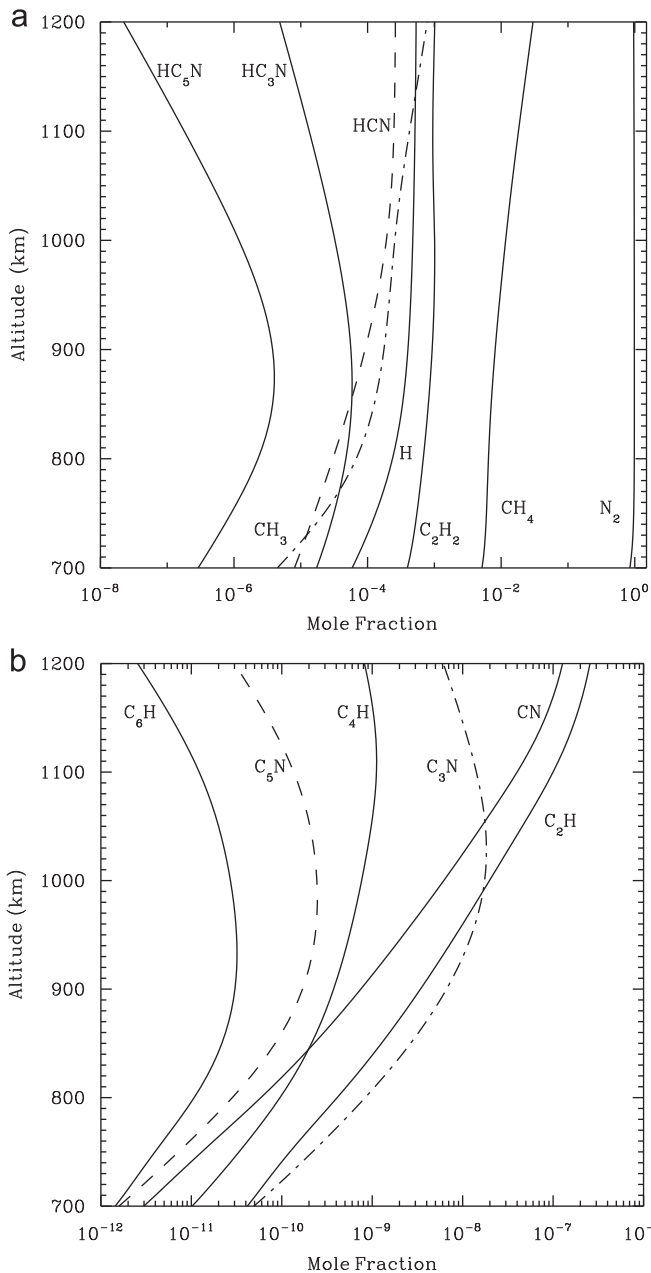


Fig. 6. Neutral species mole fraction versus altitude used as input in the ionospheric chemistry model. The same N_2 and CH_4 mole fractions are used in the photoelectron model. The way these profiles have been retrieved is described in the text and in Table 4.

reaction list are given in Fig. 7. At the negative ion density peak, located around 1050 km, the total negative ion density reaches a magnitude of $\sim 1 \text{ cm}^{-3}$. This is a quite small abundance of negative ions, about 1/1000 of the total positive ion density. The altitude of the peak for individual ions varies from ~ 800 to ~ 1100 km, depending on the dominant production/loss processes and the scale height of the parent molecule.

CN^- and C_3N^- are the two most prominent ions around 1000 km, with densities of ~ 1 and $\sim 0.2 \text{ cm}^{-3}$, respectively. C_5N^- becomes the most abundant ion below ~ 850 km, because of the larger scale height of HC_5N . The anions issued from polyyne species, C_4H^- and C_6H^- , also contribute to the total ion density at lower altitude. The density of the other ions is negligible ($< 2 \times 10^{-3} \text{ cm}^{-3}$) at all altitudes.

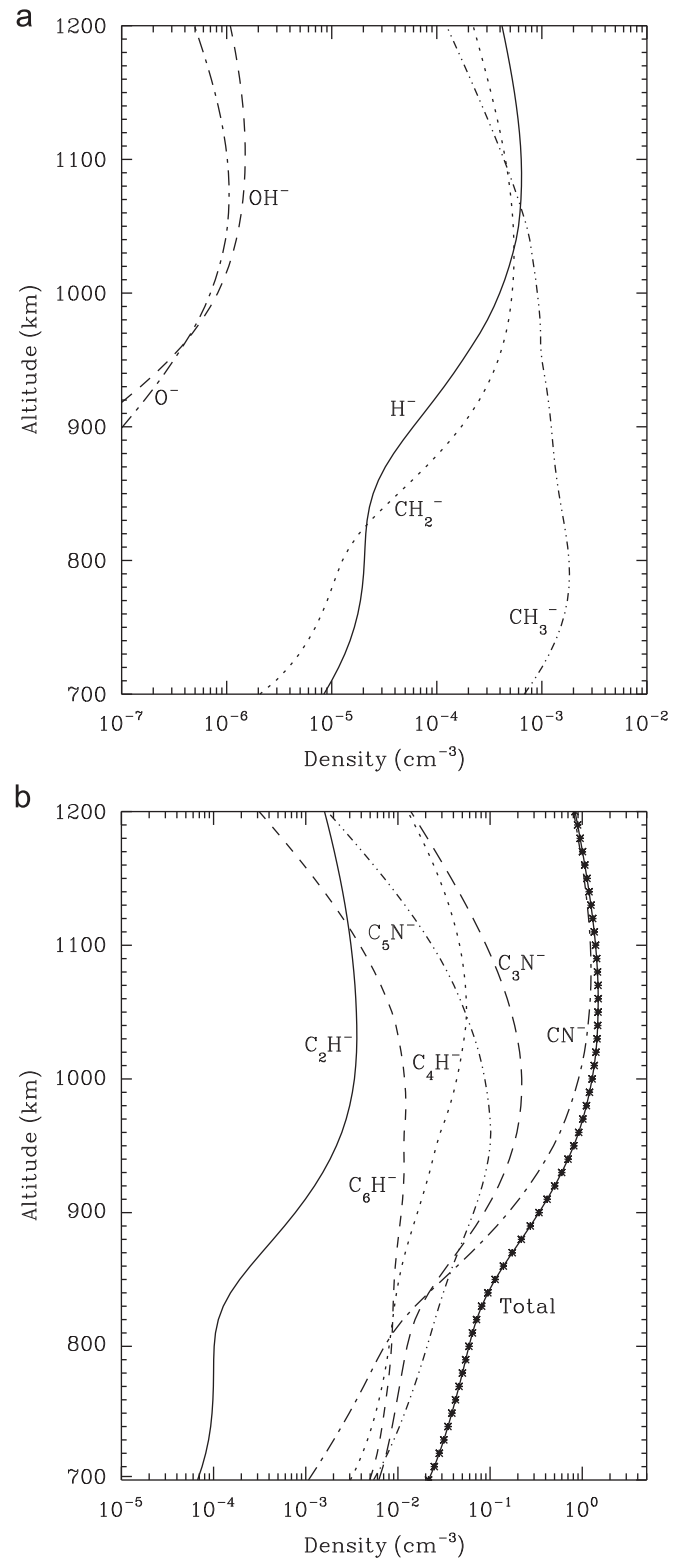


Fig. 7. Negative ions density versus altitude as calculated by the ionospheric chemistry model.

At higher altitude, negative ion production usually occurs through electron attachment and at lower altitude, proton exchange reactions of the ions with more acidic neutrals tend to dominate the loss and production of the ions. Loss occurs mostly through associative detachment with radicals (H , CH_3) throughout the ionosphere with recombination with positive ions

and photo-detachment becoming progressively more important as the altitude increases. The major production and loss channels for the most abundant ions CN^- and C_3N^- at 1000 km are illustrated in Fig. 8.

Throughout the ionosphere, CN^- is produced by dissociative electron attachment on HCN and HC_3N . Proton transfer of HCN to C_xH^- also contributes below 800 km. Dissociative electron attachment to other nitriles, radiative attachment to CN, and ion-pair formation are largely negligible. Associative detachment with H and CH_3 is responsible for most of the CN^- destruction. Proton transfer of HC_3N to CN^- also contributes at lower altitude while the contribution of photo-detachment becomes more important in the upper ionosphere. Recombination with positive ions is small for all altitudes.

For C_3N^- , proton transfer to CN^- and below 800 km, to C_xH^- is the dominant formation process. Radiative attachment to C_3N also

contributes to a lesser extent. While dissociative electron attachment is responsible for most of the CN^- formation, it is a minor mechanism for C_3N^- because of the lower cross section for HC_3N by comparison to HCN (Table 2 and Fig. 3). We could not find any cross-section for ion-pair formation from HC_3N and do not include it in the model. As discussed in the next section, the production rate associated with this process is systematically negligible for other ions and it most probably does not significantly contribute to the formation of C_3N^- either.

Similarly to CN^- , loss of C_3N^- occurs mostly through associative detachment with radicals. As shown in Table 1, we could not find any data for the gas phase acidity of HC_5N and since the EA of C_3N and C_5N are similar (4.59 ± 0.25 and 4.5 ± 0.05 eV, respectively), we do not include the proton transfer reaction from HC_5N to C_3N^- in the model. Finally, because of the high electron affinity of C_3N , photo-detachment is a minor channel, even at higher altitude.

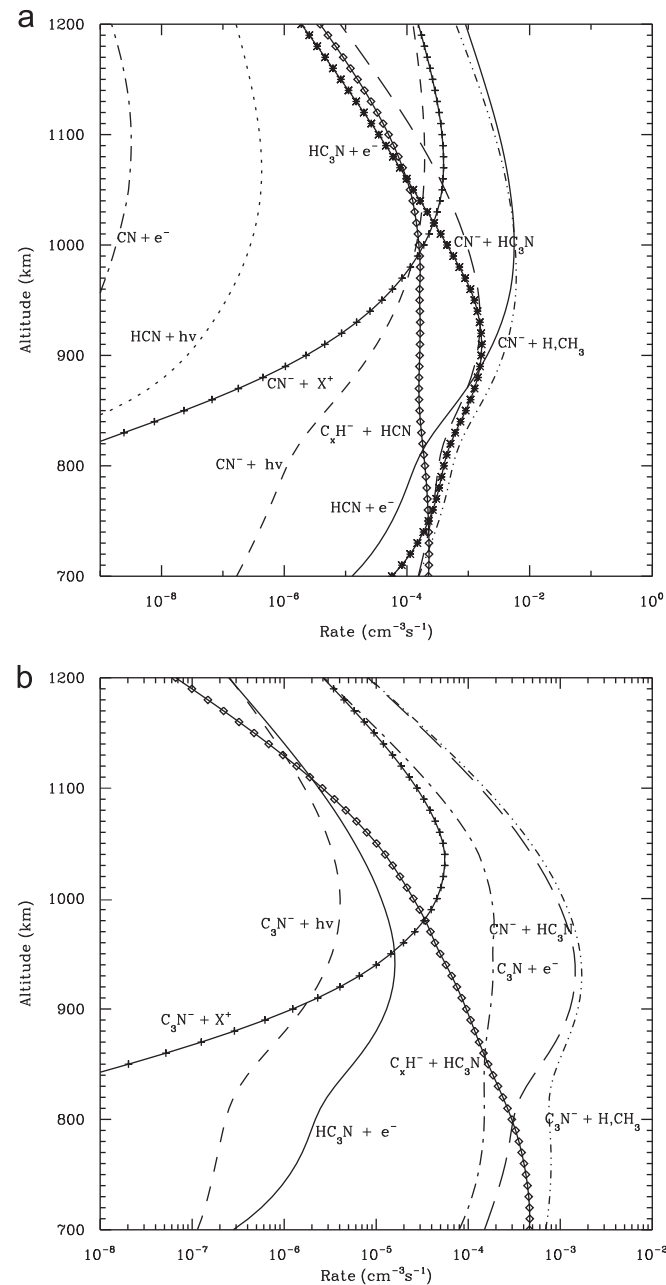


Fig. 8. Important production/destruction rates versus altitude for CN^- and C_3N^- as calculated by the ionospheric chemistry model.

6. Discussion

The ionospheric chemistry model demonstrates that two ions have a significant density ($>0.1 \text{ cm}^{-3}$) at ~ 1000 km: CN^- ($m/q = 26$) and C_3N^- ($m/q = 50$). As shown on Fig. 2, ELS detected two negative ions peaks centered at 22 ± 4 and 44 ± 8 amu/q. The uncertainty in m/q is quite large because of the finite energy width of the ELS detector, as discussed in Section 2. However, the good agreement between the model results and the observations leaves little doubt that the two main negative ions in Titan's upper atmosphere are CN^- and C_3N^- . The third most abundant ion at ~ 1000 km according to our model calculations is C_5N^- , with $m/q = 74$. The ELS spectrum presents a small peak centered at $m/q = 82 \pm 14$ that is consistent with the model prediction. Because of the increasing importance of C_4H^- over C_3N^- with altitude, C_4H^- will also contribute to the second negative ion peak for negative ions mass spectra obtained above 1100 km. C_2H^- is systematically more than two orders of magnitude less abundant than CN^- despite the fact that C_2H_2 and HCN have similar densities in the upper atmosphere (Table 4). This is due to the larger cross section for dissociative electron attachment to HCN as presented on Fig. 3.

Major sources of uncertainties for the calculated ion mole fractions arise from: (i) uncertainties in the energetic electron flux, (ii) uncertainties in the neutral vertical profiles and (iii) uncertainties in the reaction list.

The uncertainties on the description of the electron flux arise from photo-absorption, photo-ionization and electron impact cross sections (20% for ionization, up to 50% for the other processes). The uncertainties on the EUV solar flux are minor (a few percent) while the uncertainties on the X-rays are major (a factor of 2–5). However, this affects only lower altitudes (below 900 km at closest approach for T40). Finally, the thermal electron density and temperature affect the low energy supra-thermal mean intensities as well as the electron recombination rates of positive ions. They are constrained by RPWS and INMS, respectively, and represent only a minor source of uncertainty ($<20\%$).

HCN and HC_3N neutral densities are tuned to reproduce the INMS positive ion densities at 1015–1050 km (Fig. 5). Based on the Carrasco et al. (2007) sensitivity study of a Titan ionospheric model to the ion–molecule reaction parameters, Vuitton et al. (2006, 2007) estimated a factor of uncertainty of 2–5 in the neutral densities determined with this technique. Carrasco et al. (2007) sensitivity study is based on the uncertainties of measured ion–molecule reaction rates and branching ratios. However, it does not take into account the uncertainties induced by reactions that have never been studied and that are, as a consequence, lacking in

the model. The impact of these missing reactions on the inferred neutral densities is difficult to quantify but it is potentially large, especially for N-bearing species that have been poorly studied.

Cravens et al. (2009) investigated the temporal/vertical structure of Titan's night-side ionosphere in the context of the electron intensities measured by CAPS. They find that for the T5 encounter, a relative HCN abundance at 1100 km of $\sim 10^{-3}$ provides the best fit to the observed $C_2H_5^+$ and $HCNH^+$ densities, a factor of ~ 5 higher than our nominal value. This highlights the fact that a different description of the supra-thermal electron deposition, major neutral profiles, etc. can significantly affect the retrieved neutral densities.

Based on the HCN abundance retrieved by Cravens et al. (2009), we consider that an upper limit for the HCN mixing ratio of 8×10^{-4} at 1015 km is reasonable. The CN^- density increases linearly with the HCN density and with this high HCN mixing ratio, the CN^- density at 1015 km reaches 3.5 cm^{-3} . Because of proton transfer from HC_3N to CN^- , C_3N^- increases as well, to reach a density at 1015 km of 0.6 cm^{-3} .

The H and CH_3 densities control the negative ions loss through dissociative attachment reactions. Observations do not provide direct values for radicals and we have used the mole fractions calculated by the photochemical model of Lavvas et al. (2008b). This model provides a good fit to the H_2 and C_2H_6 densities measured by INMS suggesting that the calculated H and CH_3 mole fractions are probably correct within a factor of a few.

Negative ion chemistry, especially when involving N-bearing species, is extremely poorly known and potentially induces large uncertainties in the ion densities. Ion-pair formation typically amounts to $\sim 10^{-3}$ of the ionization cross-section and requires fairly high energies ($\sim 15 \text{ eV}$). Because of the sharp decrease in the solar spectrum towards shorter wavelengths, this process is systematically negligible on Titan. Photo-detachment cross sections are largely unknown but this process is only important in the very upper atmosphere. While most anion-molecule reactions considered in the model have not been studied, exothermic proton transfer and associative detachment reactions generally occur at every collision and the assumption that they occur at the Langevin rate is probably accurate within a few 10%. The same comment applies for positive-negative ion recombination. Generally, the highest source of uncertainty in the reaction list arises from cross sections for electron attachment. For CN^- , dissociative electron attachment to HCN has been characterized experimentally (Inoue, 1966) but more studies are required to confirm these results. Such studies are of the uttermost importance since electron attachment is the dominant formation process of CN^- and its density profile strongly depends on the cross sections associated with this process.

Radiative electron attachment rate coefficients, like all two-body radiative attachment rate coefficients, are extremely difficult to measure in the laboratory, and are generally evaluated via a statistical theory. With this technique, Herbst and Osamura (2008) derived the rate of radiative attachment for C_3N to be $3 \times 10^{-10} (T_e/300)^{-0.5} \text{ cm}^3 \text{ s}^{-1}$. However, from the ratio of the observed abundances of C_3N^- and C_3N in the molecular envelope of IRC+10216, Thaddeus et al. (2008) derived the same rate to be $1.9 \times 10^{-9} (T_e/300)^{-0.5} \text{ cm}^3 \text{ s}^{-1}$, on the assumption that the steady state approximation applies and photo-detachment may be neglected. This is almost an order of magnitude higher than the calculated rate. When using the rate inferred from the InterStellar Medium (ISM) observations instead of the theoretical value, our modeled C_3N^- density increases by a factor of 2 at 1000 km. This moderate increase in the C_3N^- density, relative to the difference in the applied rates, is due to the proton transfer reaction to CN^- being the dominant process controlling the C_3N^- abundance in this region.

CAPS and Magnetospheric IMaging Instrument (MIMI) onboard Cassini measured energetic O^+ ions in Saturn's outer magnetosphere (Hartle et al., 2006; Krimigis et al., 2005). Cravens et al. (2008) suggested that, when entering Titan's atmosphere, a few percent of the most energetic ions (27 keV–4 MeV) is converted to negative oxygen ions as a consequence of charge exchange

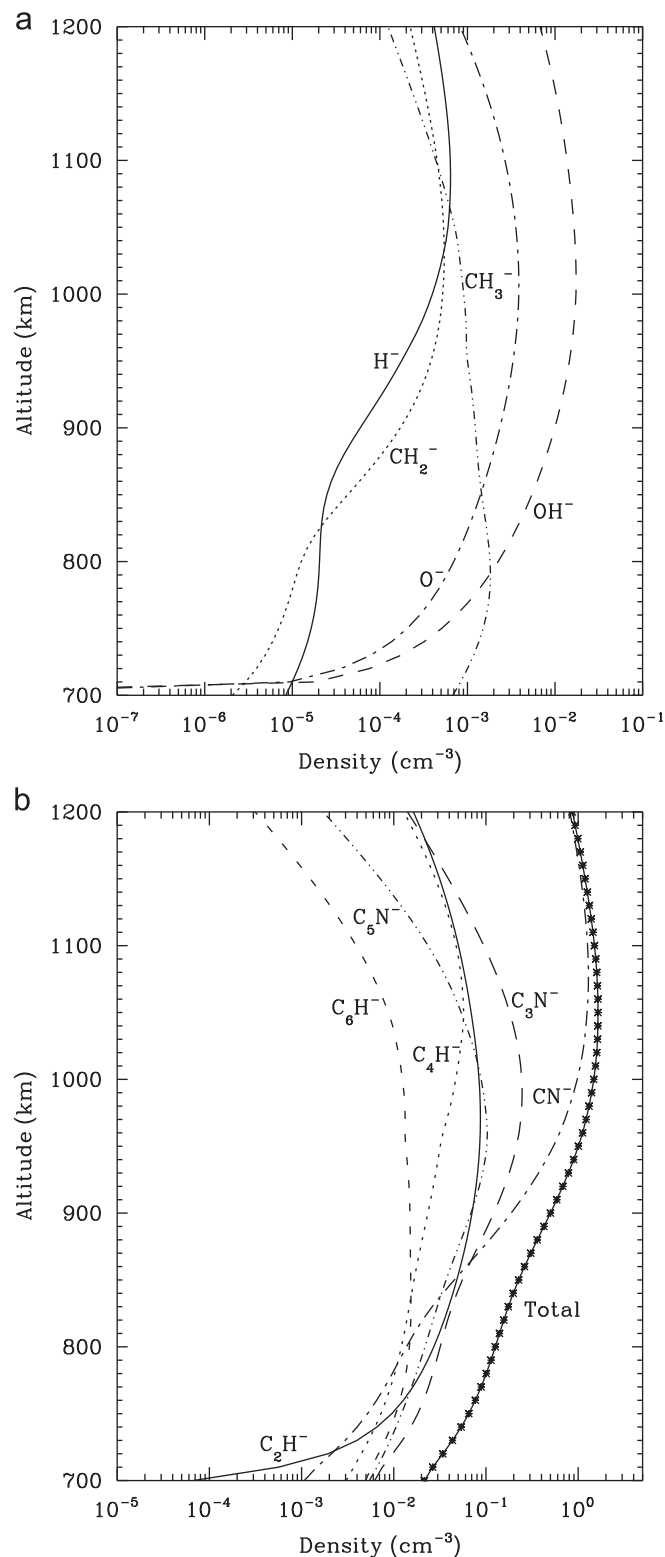


Fig. 9. Negative ions density versus altitude as calculated by the ionospheric chemistry model with an O^- flux of $10^5 \text{ cm}^{-2} \text{ s}^{-1}$.

collisions with N_2 . O^- ions would then transfer electrons to atmospheric species such as NH_3 or CH_4 , thus initiating atmospheric negative ion chemistry.

We anticipate that the fraction of O^- in the beam is likely to be smaller than calculated by Cravens et al. (2008). The lack of cross section data at low energy makes estimating the O^- fraction difficult. Cravens et al. (2008) used cross sections at ~ 1 keV, the lowest energy available, for their estimates of the O^- , but the determining factor for the final state of the incident ions are the cross sections at tens of eV. Until these cross sections are available we can only say that the O^- fraction should be between negligible and the $\sim 5\%$ estimated by Cravens et al. (2008).

In order to test the O^- hypothesis, we added a flux of O^- in our ionospheric chemistry model of $10^5 \text{ cm}^{-2} \text{ s}^{-1}$, corresponding to 5% of the “typical” Cassini MIMI case presented in the Fig. 1 of Cravens et al. (2008). The altitude of deposition is centered at 900 km based on their Fig. 3. Because of its strong basicity, O^- can subsequently proton exchange with a variety of neutral species to produce ions such as $C_{2n}H^-$, CN^- and C_3N^- , as detailed in Table 3. The retrieved ion vertical profiles are shown on Fig. 9. With this O^- flux, the O^- density increases by $\sim 10^4$ at the peak, reaching $2 \times 10^{-2} \text{ cm}^{-3}$. This essentially translates into higher densities for OH^- and C_2H^- (4×10^{-3} and 8×10^{-2} at 1015 km, respectively). CN^- and C_3N^- are only slightly affected because the production rate from the other processes described previously still dominates. We conclude that the O^- flux suggested by Cravens et al. (2008), even if real, cannot account for the negative ion densities measured by CAPS-ELS.

Four negative ions have been detected so far in the interstellar medium: C_4H^- (Cernicharo et al., 2007), C_6H^- (McCarthy et al., 2006), C_8H^- (Brünken et al., 2007; Remijan et al., 2007) and C_3N^- (Thaddeus et al., 2008). The ratio of the abundance of these 4 ions to the corresponding radical is presented in Table 5. This ratio decreases in the following order: $C_8H^-/C_8H > C_6H^-/C_6H > C_3N^-/C_3N > C_4H^-/C_4H$, with a value of 3×10^{-1} for the first pair down to 3×10^{-4} for the last one. By comparison, at the negative ion peak on Titan, we find $CN^-/CN > C_3N^-/C_3N \sim C_5N^-/C_5N$ and $C_6H^-/C_6H > \sim C_4H^-/C_4H > C_2H^-/C_2H$, with values ranging from $\sim 10^{-2}$ to $\sim 10^{-5}$.

It is striking that for a common ion, the ion/radical ratios are very similar in both environments. In the interstellar medium, radiative electron attachment to open-shell species is believed to be the main mechanism leading to negative ions. Loss occurs through association with H atoms and neutralization with positive ions. We find that the same mechanisms govern the C_4H^- and C_6H^- densities below 1200 km on Titan, except that recombination with positive ions is negligible. Because radiative electron attachment is proportional to $T^{-0.5}$, higher electron temperature on Titan (close to 1000 K) and smaller electron to atomic hydrogen densities ($\sim 10^{-4}$ at 1000 km) explain the small difference in ion to radical density found on Titan compared to the ISM.

Table 5
Negative ion/radical density ratio in Titan's ionosphere and the molecular envelope of IRC+10216.

	Titan	IRC+10216
C_2H^-/C_2H	2.4×10^{-5}	–
C_4H^-/C_4H	1.6×10^{-4}	2.6×10^{-4}
C_6H^-/C_6H	4.7×10^{-2}	6.2×10^{-2}
C_8H^-/C_8H	–	$(2.6\text{--}3.6) \times 10^{-1}$
CN^-/CN	1.9×10^{-2}	–
C_3N^-/C_3N	1.9×10^{-3}	5.2×10^{-3}
C_5N^-/C_5N	3.5×10^{-3}	–

For Titan, the ratios are taken at the maximum of the negative ion density. For IRC+10216, the ratios are from Thaddeus et al. (2008) and references therein.

7. Conclusion

We developed the first negative ion chemistry model of Titan's upper atmosphere. We determined the production and loss processes for 11 negative ions constituted of C, H, O and N. We found that the total negative ion density reaches 1 cm^{-3} but that it is sensitive to the supra-thermal electron intensities, neutral densities and chemical kinetics. A sensitivity analysis similar to the work performed for positive ion chemistry by Carrasco et al. (2007) would be valuable. It would be especially interesting to show in more detail which rate data are most needed and with what accuracy.

The two major peaks detected by ELS at $m/q = 22 \pm 4$ and 44 ± 8 are identified as CN^- and C_3N^- . A smaller peak observed at $m/q = 82 \pm 14$ is likely due to C_5N^- . Ions with a polyene-like structure (C_4H^- and C_6H^-) are also fairly abundant (up to 5×10^{-2} and 10^{-2} cm^{-3} , respectively) and contribute significantly to the total ion density below 800 km. Above 1100 km, C_4H^- and C_3N^- densities are comparable and both ions contribute to the ELS negative ion peak centered at 44 ± 8 amu.

The CAPS-ELS detectors were designed to measure electrons, not negative ions, as these were not expected in Titan's upper atmosphere as detailed in the introduction. The instrument response was therefore not calibrated in the laboratory for ions, and hence the micro-channel plate efficiency can only be estimated based on nominal ion efficiencies. Better characterization of the detectors is under way and a quantitative comparison of the calculated negative ion densities to the observations will be presented in a subsequent paper.

Observation of a large abundance of negatively charged aerosols does not necessarily implies that chemical growth occurs through negative ion chemistry, as particles could attach electrons after having already reached a substantial size. In Titan's cold environment, only exothermic reactions with a small energy barrier ($< 2 \text{ kJ mol}^{-1}$) can take place. This is generally the case for reactions involving either positively or negatively charged ions. Another possibility is the chemistry driven by highly energetic radicals, which proceeds efficiently even at the lowest temperatures (Smith et al., 2006). Finally, radical–radical reactions are a third possibility. In the thermosphere, the pressure is too low for 3-body reactions to occur but it is possible that radiative emission releases the excess energy associated with the recombination (Klippenstein, personal communication).

Determining which of these processes dominates aerosol formation on Titan will require the development of chemical models that include positive and negative ion and neutral chemistry, and trace formation of molecules with masses up to a few 1000 amu. This is a daunting task because of the huge number of species and reactions involved. General rules describing different classes of species and reactions will have to be established. In order to do so, a good knowledge of the reaction kinetics and mechanisms is required. Data on the positive and negative ion chemistry of hydrocarbons and N-bearing species as well as on the radiative recombination of radicals is desperately needed.

Acknowledgements

We acknowledge useful discussions with Roland Thissen, Odile Dutuit, Chris Arridge and Geraint Jones. We are very grateful to the TIMED/SEE PI, Tom Woods, and his team for providing us with the solar flux dataset and associated routines of extrapolation to planets [<http://lasp.colorado.edu/see/>].

References

- Adams, N.G., 1996. Gas phase ionic reactions. In: Drake, G.W.F. (Ed.), *Atomic, Molecular & Optical Physics Handbook*. American Institute of Physics, Woodbury, New York, pp. 441–451.
- Bakes, E.L.O., McKay, C.P., Bauschlicher, C.W., 2002. Photoelectric charging of submicron aerosols and macromolecules in the Titan haze. *Icarus* 157, 464–475.
- Barckholtz, C., Snow, T.P., Bierbaum, V.M., 2001. Reactions of C_n^- and C_nH^- with atomic and molecular hydrogen. *Astrophys. J.* 547, L171–L174.
- Bartmess, J.E., Scott, J.A., McIver, R.T., 1979. Scale of acidities in the gas phase from methanol to phenol. *J. Am. Chem. Soc.* 101, 6046–6056.
- Berkowitz, J., 1996. Photoion-pair formation. In: Becker, U., Shirley, D.A. (Eds.), *VUV and Soft X-ray Photoionization*. Plenum Press, New York, pp. 263–289.
- Berkowitz, J., Chupka, W.A., Walter, T.A., 1969. Photoionization of HCN: the electron affinity and heat of formation of CN. *J. Chem. Phys.* 50, 1497–1500.
- Bohme, D.K., 1975. The kinetics and energetics of proton transfer. In: Ausloos, P. (Ed.), *Interaction between ions and molecules*. Plenum Press, New York, USA, pp. 489–504.
- Bohme, D.K., Fehsenfeld, F.C., 1969. Thermal reactions of O^- ions with saturated hydrocarbon molecules. *Can. J. Chem.* 47, 2717–2719.
- Borucki, W.J., Levin, Z., Whitten, R.C., Keese, R.G., Capone, L.A., Summers, A.L., Toon, O.B., Dubach, J., 1987. Predictions of the electrical conductivity and charging of the aerosols in Titan's atmosphere. *Icarus* 72, 604–622.
- Borucki, W.J., Whitten, R.C., Bakes, E.L.O., Barth, E., Tripathi, S., 2006. Predictions of the electrical conductivity and charging of the aerosols in Titan's atmosphere. *Icarus* 181, 527–544.
- Botschwina, P., 1996. The two lowest electronic states of C_5N : results of coupled cluster calculations. *Chem. Phys. Lett.* 259, 627–634.
- Bradforth, S.E., Kim, E.H., Arnold, D.W., Neumark, D.M., 1993. Photoelectron spectroscopy of CN^- , NCO^- , and NCS^- . *J. Chem. Phys.* 98, 800–810.
- Brünken, S., Gupta, H., Gottlieb, C.A., McCarthy, M.C., Thaddeus, P., 2007. Detection of the carbon chain negative ion C_8H^- in TMC-1. *Astrophys. J.* 664, L43–L46.
- Capone, L.A., Dubach, J., Whitten, R.C., Prasad, S.S., Santhanam, K., 1980. Cosmic ray synthesis of organic molecules in Titan's atmosphere. *Icarus* 44, 72–84.
- Capone, L.A., Whitten, R.C., Dubach, J., Prasad, S.S., Huntress, W.T., 1976. The lower ionosphere of Titan. *Icarus* 28, 367–378.
- Carrasco, N., Dutuit, O., Thissen, R., Banaszekiewicz, M., Pernot, P., 2007. Uncertainty analysis of bimolecular reactions in Titan ionosphere chemistry model. *Planet. Space Sci.* 55, 141–157.
- Cernicharo, J., Guélin, M., Agúndez, M., Kawaguchi, K., McCarthy, M., Thaddeus, P., 2007. Astronomical detection of C_4H^- , the second interstellar anion. *Astron. Astrophys.* 467, L37–L40.
- Chupka, W.A., Dehmer, P.M., Jiverty, W.T., 1975. High resolution photoionization study of ion-pair formation in H_2 , HD, and D_2 . *J. Chem. Phys.* 63, 3929–3944.
- Coates, A.J., 2009. Interaction of Titan's ionosphere with Saturn's magnetosphere. *Phil. Trans. R. Soc. A* 367, 773–788.
- Coates, A.J., Cray, F.J., Lewis, G.R., Young, D.T., Waite, J.H., Sittler, E.C., 2007a. Discovery of heavy negative ions in Titan's ionosphere. *Geophys. Res. Lett.* 34, L22103.
- Coates, A.J., Cray, F.J., Young, D.T., Szego, K., Arridge, C.S., Bebesi, Z., Sittler, E.C., 2007b. Ionospheric electrons in Titan's tail: plasma structure during the Cassini T9 encounter. *Geophys. Res. Lett.* 34, L24505.
- Coates, A.J., Wellbrock, A., Lewis, G.R., Jones, G.H., Young, D.T., Cray, F.J., Waite, J.H., 2009. Heavy negative ions in Titan's ionosphere: altitude and latitude dependence. *Planet. Space Sci.*, this issue, doi:10.1016/j.pss.2009.05.009.
- Compton, R.N., Christophorou, L.G., 1967. Negative-ion formation in H_2O and D_2O . *Phys. Rev.* 154, 110–116.
- Cowles, D.C., Travers, M.J., Frueh, J.L., Ellison, G.B., 1991. Photoelectron spectroscopy of CH_2N^- . *J. Chem. Phys.* 94, 3517–3528.
- Cray, F., Magee, B.A., Mandt, K., Waite, J.H., Jr., Westlake, J., Young, D.T., 2009. Heavy ions in Titan's ionosphere: a comparison of Cassini CAPS and INMS observations. *Planet. Space Sci.* This issue.
- Cravens, T.E., Robertson, I.P., et al., 2006. Composition of Titan's ionosphere. *Geophys. Res. Lett.* 33, L07105.
- Cravens, T.E., Robertson, I.P., Ledvina, S.A., Mitchell, D., Krimigis, S.M., Waite, J.H., 2008. Energetic ion precipitation at Titan. *Geophys. Res. Lett.* 35, L03103.
- Cravens, T.E., Robertson, I.P., et al., 2009. Model-data comparisons for Titan's nightside ionosphere. *Icarus* 199, 174–188.
- Cravens, T.E., Vann, J., Clark, J., Yu, J., Keller, C.N., Brull, C., 2004. The ionosphere of Titan: an updated theoretical model. *Adv. Space Res.* 33, 212–215.
- Cui, J., Yelle, R.V., Vuitton, V., Waite, J.H., Kasprzak, W.T., Niemann, H.B., Gell, D., Borggren, N., Magee, B., Müller-Wodarg, I.C.F., 2009. Analysis of Titan's neutral upper atmosphere from Cassini Ion Neutral Mass Spectrometer measurements. *J. Geophys. Res.* 200, 581–615.
- Davico, G.E., Bierbaum, V.M., DePuy, C.H., Ellison, G.B., Squires, R.R., 1995. The C–H bond energy of benzene. *J. Am. Chem. Soc.* 117, 2590–2599.
- De Bleecker, K., Bogaerts, A., Goedheer, W., 2006. Detailed modeling of hydrocarbon nanoparticle nucleation in acetylene discharges. *Phys. Rev. E* 73, 026405.
- De Kok, R., Irwin, P.G., et al., 2007. Oxygen compounds in Titan's stratosphere as observed by Cassini CIRS. *Icarus* 186, 354–363.
- Deschenaux, C., Affolter, A., Magni, D., Hollenstein, C., Fayet, P., 1999. Investigations of CH_4 , C_2H_2 and C_2H_4 dusty RF plasmas by means of FTIR absorption spectroscopy and mass spectrometry. *J. Phys. D: Appl. Phys.* 32, 1876–1886.
- Dibeler, V.H., Reese, R.M., Franklin, J.L., 1961. Mass spectrometric study of cyanogen and cyanoacetylenes. *J. Am. Chem. Soc.* 83, 1813–1818.
- Ellison, G.B., Engelking, P.C., Lineberger, W.C., 1978. An experimental determination of the geometry and electron affinity of methyl radical. *J. Am. Chem. Soc.* 100, 2556–2558.
- Ervin, K.M., Gronert, S., Barlow, S.E., Gilles, M.K., Harrison, A.G., Bierbaum, V.M., Depuy, C.H., Lineberger, W.C., Ellison, G.B., 1990. Bond strengths of ethylene and acetylene. *J. Am. Chem. Soc.* 112, 5750–5759.
- Fedor, J., Cicman, P., et al., 2006. Fragmentation of transient water anions following low-energy electron capture by H_2O/D_2O . *J. Phys. B: At. Mol. Opt. Phys.* 39, 3935–3944.
- Fehsenfeld, F.C., 1975. Interaction between ions and molecules. In: Ausloos, P. (Ed.), *NATO Advanced Study Institutes Series. Series B, Physics*. Plenum Press, New York p. 387.
- Fehsenfeld, F.C., Howard, C.J., Ferguson, E.E., 1973. Thermal energy reactions of negative ions with H atoms in the gas phase. *J. Chem. Phys.* 58, 5841–5842.
- Flasar, F.M., Achterberg, R.K., et al., 2005. Titan's atmospheric temperatures, winds, and composition. *Science* 308, 975–978.
- Gal, J.-F., Decouzon, M., Maria, P.-C., González, A.I., Mó, O., Yáñez, M., El Chaouch, S., Guillemin, J.-C., 2001. Acidity trends in α,β -unsaturated alkanes, silanes, germanes, and stannanes. *J. Am. Chem. Soc.* 123, 6353–6359.
- Galand, M., Lilensten, J., Toublanc, D., Maurice, S., 1999. The ionosphere of Titan: ideal diurnal and nocturnal cases. *Icarus* 140, 92–105.
- Galand, M., Yelle, R.V., Coates, A.J., Backes, H., Wahlund, J.-E., 2006. Electron temperature of Titan's sunlit ionosphere. *Geophys. Res. Lett.* 33, L21101.
- Graupner, K., Merrigan, T.L., Field, T.A., Youngs, T.G., Marr, P.C., 2006. Dissociative electron attachment to HCCCN. *New J. Phys.* 8, 117–133.
- Gunion, R.F., Gilles, M.K., Polak, M.L., Lineberger, W.C., 1992. Ultraviolet photoelectron spectroscopy of the phenide, benzyl, and phenoxide anions, with ab initio calculations. *Int. J. Mass Spectrom. Ion Proc.* 117, 601–620.
- Hartle, R.E., Sittler, E.C., et al., 2006. Initial interpretation of Titan plasma interactions as observed by the Cassini Plasma Spectrometer: comparisons with Voyager 1. *Planet. Space Sci.* 54, 1211–1224.
- Haxton, D.J., Rescigno, T.N., McCurdy, C.W., 2007. Dissociative electron attachment to the H_2O molecule. II. Nuclear dynamics on coupled electronic surfaces within the local complex potential model. *Phys. Rev. A* 75, 012711.
- Heni, M., Illenberger, E., 1986. Electron attachment by saturated nitriles, acrylonitrile (C_3H_3CN) and benzonitrile (C_6H_5CN). *Int. J. Mass Spectrom. Ion Process.* 73, 127–144.
- Herbst, E., Osamura, Y., 2008. Calculations of the formation rates and mechanisms for C_nH anions in interstellar and circumstellar media. *Astrophys. J.* 679, 1670–1679.
- Hickman, A.P., 1979. Approximate scaling formula for ion–ion mutual neutralization rates. *J. Chem. Phys.* 70, 4872–4878.
- Hotop, H., Lineberger, W.C., 1985. Binding energies in atomic negative ions: II. *J. Phys. Chem. Ref. Data* 14, 731–750.
- Howard, C.J., Fehsenfeld, F.C., McFarland, M., 1974. Negative ion–molecule reactions with atomic hydrogen in the gas phase at 296 °K. *J. Chem. Phys.* 60, 5086–5089.
- Howling, A.A., Sansonnens, L., Dorier, J.-L., Hollenstein, C., 1994. Time-resolved measurements of highly polymerized negative ions in radio frequency silane plasma deposition experiments. *J. Appl. Phys.* 75, 1340–1353.
- Hörst, S.M., Vuitton, V., Yelle, R.V., 2008. The origin of oxygen species in Titan's atmosphere. *J. Geophys. Res.* 113, E10006.
- Inoue, M., 1966. Ions négatifs formés dans le cyanogène et l'acide cyanhydrique. *J. Chim. Phys. Physico-Chim. Biol.* 63, 1061–1071.
- Kass, S.R., DePuy, C.H., 1985. Gas phase ion chemistry of azides. The generation of $CH=N^-$ and $CH_2=NCH_2^-$. *J. Org. Chem.* 50, 2874–2877.
- Kim, Y.-K., Irikura, K.K., 2000. In: *Proceedings of the 2nd International Conference on Atomic and Molecular Data and their Applications*. AIP, New York, p. 543, 20.
- Krimigis, S.M., Mitchell, D.G., et al., 2005. Dynamics of Saturn's magnetosphere from MIMI during Cassini's orbital insertion. *Science* 307, 1270–1273.
- Lara, L.M., Lellouch, E., Lopez-Moreno, J.J., Rodrigo, R., 1996. Vertical distribution of Titan's atmospheric neutral constituents. *J. Geophys. Res.* 101, 23261–23283.
- Lavvas, P., Coustenis, A., Vardavas, I.M., 2008a. Coupling photochemistry with haze formation in Titan's atmosphere. Part I: Model description. *Planet. Space Sci.* 56, 27–66.
- Lavvas, P., Coustenis, A., Vardavas, I.M., 2008b. Coupling photochemistry with haze formation in Titan's atmosphere. Part II: Results and validation with Cassini/Huygens data. *Planet. Space Sci.* 56, 67–99.
- Lavvas, P., Yelle, R.V., Vuitton, V., 2009. The detached haze layer in Titan's mesosphere. *Icarus* 201, 626–633.
- Lebonnois, S., Bakes, E.L.O., McKay, C.P., 2002. Transition from gaseous compounds to aerosols in Titan's atmosphere. *Icarus* 159, 505–517.
- Leopold, D.G., Murray, K.K., Stevens Miller, A.E., Lineberger, W.C., 1985. Methylene: a study of the X^3B_1 and \tilde{a}^1A_1 states by photoelectron spectroscopy of CH_2 and CD_2 . *J. Chem. Phys.* 83, 4849–4865.
- Lequeux, J., 2005. *The Interstellar Medium*. Springer, Berlin.
- Linder, D.R., Coates, A.J., 8 colleagues, 1998. The Cassini CAPS electron spectrometer. In: Pfaff, R.E., et al. (Eds.), *Measurement Techniques in Space Plasmas: Particles*. AGU Geophysical Monograph, pp. 257–262.
- Mackay, G.I., Betowski, L.D., Payzant, J.D., Schiff, H.I., Bohme, D.K., 1976. Rate constant at 297 K for proton-transfer reactions with hydrocyanic acid and acetonitrile. Comparisons with classical theories and exothermicity. *J. Phys. Chem.* 80, 2919–2922.

- Mackay, G.I., Tanaka, K., Bohme, D.K., 1977. Rate constants at 297 K for proton-transfer reactions with C_2H_2 : an assessment of the average quadrupole orientation theory. *Int. J. Mass Spectrom. Ion Phys.* 24, 125–136.
- McCarthy, M.C., Gottlieb, C.A., Gupta, H., Thaddeus, P., 2006. Laboratory and astronomical identification of the negative molecular ion C_6H^- . *Astrophys. J.* 652, L141–L144.
- Millar, T.J., Walsh, C., Cordiner, M.A., Chuimin, R.N., Herbst, E., 2007. Hydrocarbon anions in interstellar clouds and circumstellar envelopes. *Astrophys. J.* 662, L87–L90.
- Mitsuke, K., Suzuki, S., Imamura, T., Koyano, I., 1991. Negative-ion mass spectro-metric study of ion-pair formation in the vacuum ultraviolet. IV. $CH_4 \rightarrow H^- + CH_3^+$ and $CD_4 \rightarrow D^- + CD_3^+$. *J. Chem. Phys.* 94, 6003–6006.
- Molina-Cuberos, G.J., López-Moreno, J.J., Rodrigo, R., 2000. Influence of electro-philic species on the lower ionosphere of Titan. *Geophys. Res. Lett.* 27, 1351–1354.
- Moran, S., Ellis, H.B., DeFrees, D.J., McLean, A.D., Ellison, G.B., 1987. Carbanion spectroscopy: cyanomethide anion (CH_2CN^-). *J. Am. Chem. Soc.* 109, 5996–6003.
- Oertel, H., Schenk, H., Baumgärtel, H., 1980. Ion pair formation from photon irradiation of O_2 , NO and CO in 17–30 eV. *Chem. Phys.* 46, 251–262.
- Perrin, J., Böhm, C., Etemadi, R., Lloret, A., 1994. Possible routes for cluster growth and particle formation in RF silane discharges. *Plasma Sources Sci. Technol.* 3, 252–261.
- Petrie, S., 1996. Novel pathways to CN^- within interstellar clouds and circumstellar envelopes: implications for IS and CS chemistry. *Mon. Not. R. Astron. Soc.* 281, 137–144.
- Petrie, S., Herbst, E., 1997. Some interstellar reactions involving electrons and neutral species: Attachment and isomerization. *Astrophys. J.* 491, 210–215.
- Raksit, A.B., Bohme, D.K., 1983. An experimental study of the influence of hydration on the reactivity of the hydroxide anion in the gas phase at room temperature. *Can. J. Chem.* 61, 1683–1689.
- Rapp, D., Briglia, D.D., 1965. Total cross sections for ionization and attachment in gases by electron impact. II. Negative-ion formation. *J. Chem. Phys.* 43, 1480–1489.
- Remijan, A.J., Hollis, J.M., Lovas, F.J., Cordiner, M.A., Millar, T.J., Markwick-Kemper, A.J., Jewell, P.R., 2007. Detection of C_8H^- and comparison with C_8H toward IRC +10216. *Astrophys. J.* 664, L47–L50.
- Ruscic, B., Berkowitz, J., 1990. Photoion-pair formation and photoelectron-induced dissociative attachment in C_2H_2 : $D_0(HCC-H)$. *J. Chem. Phys.* 93, 5586–5593.
- Rutkowski, J., Drost, H., Spangenberg, H.-J., 1980. Investigation of the inelastic interaction of slow monoenergetic electrons with simple hydrocarbon molecules. *Ann. Phys.* 7, 259–270.
- Sailer, W., Pelc, A., Limão-Vieira, P., Mason, N.J., Limtrakul, J., Scheier, P., Probst, M., Märk, T.D., 2003. Low energy electron attachment to CH_3CN . *Chem. Phys. Lett.* 381, 216–222.
- Schulz, P.A., Mead, R.D., Jones, P.L., Lineberger, W.C., 1982. OH^- and OD^- threshold photodetachment. *J. Chem. Phys.* 77, 1153–1165.
- Sharp, T.E., Dowell, J.T., 1967. Isotope effects in dissociative attachment of electrons in methane. *J. Chem. Phys.* 46, 1530–1531.
- Shiell, R.C., Hu, X., Hu, I.J., Hepburn, J.W., 2000. Threshold ion-pair production spectroscopy (TIPPS) of H_2 and D_2 . *Faraday Discuss.* 115, 331–343.
- Smith, D., Church, M.J., Miller, T.M., 1978. Mutual neutralization of simple and clustered positive and negative ions. *J. Chem. Phys.* 68, 1224–1229.
- Smith, I.W., Sage, A.M., Donahue, N.M., Herbst, E., Quan, D., 2006. The temperature-dependence of rapid low temperature reactions: experiment, understanding and prediction. *Faraday Discuss.* 133, 137–156.
- Stamatovic, A., Schulz, G.J., 1970. Dissociative attachment in CO and formation of C^- . *J. Chem. Phys.* 53, 2663–2667.
- Taft, R.W., Abboud, J.L., et al., 1988. Regarding the inherent dependence of resonance effects of strongly conjugated substituents on electron demand. *J. Am. Chem. Soc.* 110, 1797–1800.
- Taylor, T.R., Xu, C., Neumark, D.M., 1998. Photoelectron spectra of the $C_{2n}H^-$ ($n = 1-4$) and $C_{2n}D^-$ ($n = 1-3$) anions. *J. Chem. Phys.* 108, 10018–10026.
- Teanby, N.A., Irwin, P.G., et al., 2006. Latitudinal variations of HCN, HC_3N , and C_2N_2 in Titan's stratosphere derived from Cassini CIRS data. *Icarus* 181, 243–255.
- Thaddeus, P., Gottlieb, C.A., Gupta, H., Brünken, S., McCarthy, M.C., Agúndez, M., Guélin, M., Cernicharo, J., 2008. Laboratory and astronomical detection of the negative molecular ion C_3N^- . *Astrophys. J.* 677, 1132–1139.
- Toublanc, D., Parisot, J.P., Brillet, J., Gautier, D., Raulin, F., McKay, C.P., 1995. Photochemical modeling of Titan's atmosphere. *Icarus* 113, 2–26.
- Tsuda, S., Yokohata, A., Umaba, T., 1973. Measurement of negative ions formed by electron impact. IX. Negative ion mass spectra and ionization efficiency curves of negative ions of m/e 25, 26, 27, 38, 39, 40 and 50 from acrylonitrile. *Bull. Chem. Soc. Japan* 46, 2273–2277.
- Viggiano, A.A., Paulson, J.F., 1983. Temperature dependence of associative detachment reactions. *J. Chem. Phys.* 79, 2241–2245.
- Vinatier, S., Bézard, B., et al., 2007. Vertical abundance profiles of hydrocarbons in Titan's atmosphere at 15°S and 80°N retrieved from Cassini/CIRS spectra. *Icarus* 188, 120–138.
- Vuitton, V., Yelle, R.V., Anicich, V.G., 2006. The nitrogen chemistry of Titan's upper atmosphere revealed. *Astrophys. J.* 647, L175–L178.
- Vuitton, V., Yelle, R.V., Cui, J., 2008. Formation and distribution of benzene on Titan. *J. Geophys. Res.* 113, E05007.
- Vuitton, V., Yelle, R.V., McEwan, M.J., 2007. Ion chemistry and N-containing molecules in Titan's upper atmosphere. *Icarus* 191, 722–742.
- Waite, J.H., Young, D.T., Cravens, T.E., Coates, A.J., Crary, F.J., Magee, B., Westlake, J., 2007. The process of tholin formation in Titan's upper atmosphere. *Science* 316, 870–875.
- Wickham-Jones, T., Ervin, K.M., Ellison, G.B., Lineberger, W.C., 1989. NH_2 electron affinity. *J. Chem. Phys.* 91, 2762–2763.
- Wilson, E.H., Atreya, S.K., 2003. Chemical sources of haze formation in Titan's atmosphere. *Planet. Space Sci.* 51, 1017–1033.
- Woods, T.N., 2008. Recent advances in the observations and modeling of the solar ultraviolet and X-ray spectral irradiance. *Adv. Space Res.* 42, 895–902.
- Woods, T.N., Eparvier, F.G., Bailey, S.M., Chamberlin, P.C., Lean, J., Rottman, G.J., Solomon, S.C., Tobiska, W.K., Woodraska, D.L., 2005. Solar EUV Experiment (SEE): Mission overview and first results. *J. Geophys. Res.* 110, A01312.
- Yelle, R.V., Borggren, N., De La Haye, V., Kasprzak, W.T., Niemann, H.B., Müller-Wodarg, I.C.F., Waite, J.H., 2006. The vertical structure of Titan's upper atmosphere from Cassini Ion Neutral Mass Spectrometer measurements. *Icarus* 182, 567–576.
- Young, D.T., Berthelier, J.-J., et al., 2004. Cassini plasma spectrometer investigation. *Space Sci. Rev.* 114, 1–112.
- Yung, Y.L., Allen, M., Pinto, J.P., 1984. Photochemistry of the atmosphere of Titan: comparison between model and observations. *Astrophys. J. Suppl. Ser.* 55, 465–506.